IEEE Access
Multidisciplinary | Rapid Review | Open Access Journal

Received 5 November 2023, accepted 20 November 2023, date of publication 21 November 2023,
date of current version 29 November 2023.

Digital Object Identifier 10.1109/ACCESS.2023.3335814

RESEARCH ARTICLE

Analysis of Influence Factors of Guide Vanes Torque in Variable Geometry Turbine Adjusting Mechanism

YAN ZHONG, LIANGYU CHEN, LEI ZHAO, LEI WANG, ZHUO YAN, AND HAOXI BAI
School of Mechanical Engineering and Automation, Northeastern University, Shenyang 110819, China

Corresponding author: Liangyu Chen (chenly405@163.com)

This work was supported by the Cooperation Project between the National Key Aero-Engine Research Institute and Northeastern University under Grant 2018JX03H002.

ABSTRACT More and more attention has been paid to research on variable geometry turbine engines with the increasing improvement of performance requirements for military turbines. Due to the fixed working angle of the inlet guide vane, the performance of a conventional fixed geometry turbine is optimal only for turbines near the design point. To match the aircraft's starting, climbing, cruising, deceleration, landing and other working states, it is necessary to change the turbine speed. This will not only reduce the performance of the turbine but also increase the fuel loss. The variable geometry turbine is a perfect solution to this problem. It is not necessary to change the speed of the turbine, but only the working angle of the inlet rotating guide vane of the turbine. The variable geometry turbine can be matched to each state of the aircraft's entire voyage. The turbine guide vane can be adjusted by 7° to bring about a 10% change in the flow rate of the entire machine. With constant turbine inlet temperature, the fuel loss can be effectively reduced. The rotating guide vane is impacted by the high-temperature and high-pressure gas and cold air in the inner culvert. Hot and cold air produce two types of aerodynamic torque on the rotating guide vane. There is also a friction torque on the rotating shaft of the guide vane. Therefore, the rotating guide vanes of variable geometry turbines are subjected to three types of torques. The main objective of this paper is to study three factors influencing the guide vane torque in the main flow path. The three influencing factors are the turbulence intensity of the gas, the flow ratio of cold gas to hot gas and the location distribution of the gas film holes on the guide vane. In this paper, CFD temperature-fluid-solid coupling algorithm combined with UDF program is applied to solve the torque of guide vane shaft at three influencing factors. The results show that the three factors, turbulence intensity, flow ratio and air film hole distribution, can have a significant effect on the guide vane torque. This is of great significance for the research and design of variable geometry turbines.

INDEX TERMS Turbulence intensity, flow ratio, air film hole distribution, temperature-fluid-solid coupling algorithm, UDF program, rotating guide vane torque, deflection angle, variable geometry turbine.

I. INTRODUCTION

The conventional engine turbine guide structure is a static annular cascade composed of inner rings and outer rings and a set of guide vanes. Generally, it is fixed on the turbine casing by the outer ring. Figure 1 shows the turbine structure of a conventional engine. The gas will flow out of the convergent channel of the guide vanes. The speed will increase. Pressure and temperature will drop. The direction of the air flow will also change. Therefore, the function of the deflector is to convert part of the heat energy of the air flow into kinetic energy. And the air flows out in a certain direction. The gas pushes the working wheel to do work [1].

The fixed geometry turbine engine has two main problems. First, there is the best thermodynamic performance only near the design state. Second, the thrust of each state is obtained

The associate editor coordinating the review of this manuscript and approving it for publication was Jingang Jiang.

by adjusting the speed. It will cause the flow mismatch of the propulsion system. And intake and exhaust losses will also increase [1].

At present, the use of military fighter is becoming more and more complex with the harsh demands of modern war. The takeoff and landing distances become shorter. The voyage becomes farther. Mobility becomes stronger. The characteristics of sustainable supersonic cruise are outstanding. Conventional turbine engines can no longer fully meet the needs of future fighters. Therefore, all countries are committed to the exploration, research and verification of variable cycle engines. The variable cycle engine has obvious improvement in the above two aspects. Under different flight conditions, it can improve the thermodynamic cycle of maximum thrust state. It can increase thrust. It can improve the flow matching of the propulsion system. It can improve the acceleration and deceleration of the engine. It can improve and adjust the matching relationship between components. The candidate engine F120 of the American F22 fighter is a variable cycle engine [2].

The variable geometry turbine is a key component of a variable cycle engine. Variable geometry turbines have been studied at home and abroad. The adjustable guide vane angle is a main way to realize the variable geometry turbine. It is also the main research direction of the variable geometry turbine at present. The design idea is to install a set of mechanical adjustment mechanism on the outside of the engine casing. The guide vane is driven to rotate by the adjusting mechanism. Through the rotation of the guide vane, the working angle of the guide vane is changed. It changes the exhaust area of the turbine guide structure. It realizes the adjustment of the work distribution between the high pressure rotor and the low pressure rotor. Its main feature is to change the flow matching between the moving blade and the guide vane in the turbine. The air flow area in the turbine passage is changed. The overall working performance of the turbine is improved [3]. Figure 2 shows the variable geometry engine turbine structure.

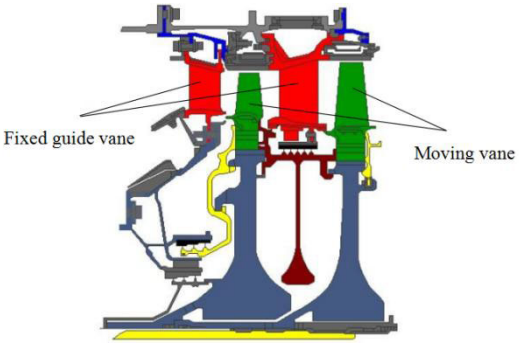

FIGURE 1. Turbine structure of conventional engine.

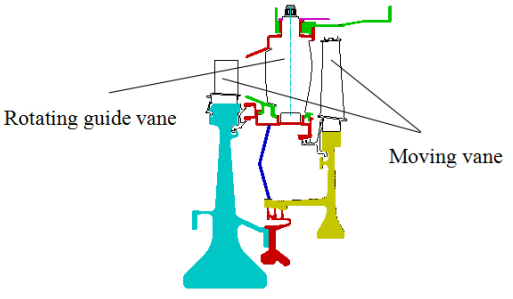

FIGURE 2. Turbine structure of variable geometry engine.

In recent years, variable cycle engines have been a new development direction for turbines. Rotating guide vanes and variable geometry structures were the main research directions. In order to obtain the best engine performance and ensure the stability of the compressor, Li and Wang [4] proposed a PID controller based on iterative learning, which used Iterative learning control to perform the desired trajectory tracking control. Simulation results showed that the designed controller could achieve the guide vane angle actuator displacement regulator of rapid, accurate track, indicating that the controller design method was feasible and effective. Zhao et al. [5] focused on the application of multi-objective optimization methods in the three-parameter two-stage closure law. When the unit suddenly rejected load, it effectively coordinated the contradiction between increasing speed and increasing hydrodynamic pressure. Obretenov and Iliev [6] presented the results of an experimental study of a Darrieus type vertical wind turbine. The characteristics of the turbine had been investigated and the optimal values of three of the parameters had been determined with planned physical experiment: pitch angle of the working blades, pitch angle of the guide vanes and number of the guide vanes. Anantharkrishnan and Govardhan [7] studied the effect of constant and variable radius fillets on the secondary flow loss of transonic turbine stage nozzle guide vanes. The results were discussed using the topological characteristics of the flow field, Mach number, and density contour lines. Increment in leading edge radius increased the movement of these flows towards midspan while the effect of minimum angle was found to be insignificant. Kukutla and Prasad [8] obtained the flow analysis of nozzle guide blades under the action of thermal mainstream by conducting three-dimensional calculations and analysis on the nozzle guide blades. The results showed that for the combination of coolant mass flow rate and mainstream Reynolds number, there was the possibility of local optimization solutions. Peng et al. [9] studied the application of improved genetic algorithm in parameter optimization of a certain aircraft engine compressor guide vane regulator. The results showed that the improved genetic algorithm had advantages such as global search and fast evolution. The ultimate guide vane regulator formed through semiphysical simulation had good static and dynamic characteristics. Nižetić et al. [10] studied the effects of different blade shapes (geometric changes) and different attack angle configurations on vortex stability and shape. The results showed that geometric modifications had a significant impact on the minimal required delta pressure required to establish

and maintain eddies. Hu et al. [11] established the basic parametric equation of the combined drive system of the rotating guide rod and gear mechanism of the differential vane pump, and analyzed its kinematics characteristics. Gupta et al. [12] presented a novel magnetically levitated vertical axis wind turbine (VAWT) with omni-directional guide vanes which acted as wind concentrator as well as wind shield. The vanes protected the turbine from high velocity winds and increased its performance under low velocity winds. Zhang et al. [13] mainly focused on understanding the dynamic behavior of pump turbine in the small guide vanes opening based on numerical simulations. During the data analysis, special attention had been paid to the pressure fluctuation within pump turbine. Ding et al. [14] studied the heat transfer distribution on the surface of two internally cooled nozzle guide vanes in a transonic annular cascade. The effects of outlet Mach number on heat transfer of nozzle guide vanes were also studied.

Variable geometry compressors were easier to achieve variable cycle performance compared to turbines. Because compressors did not need to consider the effects of high-temperature thermal deformations and flexible bodies, this was significantly different from variable geometry turbines. In order to overcome the shortcomings of casing treatment, Cheng and Sakaguchi [15] proposed an application of processing 14 three-dimensional guide vanes inside the casing. Numerical results showed that the optimized guide vanes held a possibility to improve off-design performance by reducing the excessive pre-whirl at the compressor inlet. Xu et al. [16] used FLUENT software to numerically simulate the internal flow field and external characteristics of two guide vane models. The external characteristic comparison showed that under the rated condition, the efficiency of the pump installed with the axial guide vane was 8.9% higher than that of the radial one. The comparative analysis of the internal flow field of the two guide vanes revealed that the axial guide vane could effectively improve the internal flow pattern and obtain better hydraulic performance. By utilizing the blade position and shaft speed of variable geometry turbochargers, Zeng et al. [17] developed a physics based turbine power and power loss model. The proposed model was validated against a few sets of test data from both steady state and transient operations. Ye and Zhu [18] analyzed the proportion of eddy current energy loss to theoretical boost in axial flow fans of domestically produced 300MW and Westinghouse 135MW generators. The results both of the CFD numerical simulation and model-testing proved that the straightener vanes could change 90% of the swirl energy losses into the useful energy, they could improve the efficiency of the fan about 12.33% compared with the same fan without guide vanes. Tong and Tong [19] conducted heat transfer experiments on the turbine guide vanes of a certain type of aircraft engine and numerically simulated the gas thermal coupling using CFX. At the same time, the improvement of the aerodynamic heat transfer calculation of the high-pressure turbine guide vane provided a numerical calculation for the numerical simulation of the heat transfer of the blade air-cooled structure. Zhao et al. [20] used ANSYS CFX software to calculate and analyze the pressure fluctuations of the impeller and guide vanes of the boiler water circulation pump. The results showed that: with the increase of the flow rate, the periodicity of pressure fluctuations at monitoring points in the impeller and the guide vane became more and more obvious, and the fluctuation amplitude decreased gradually. Xiao et al. [21] proposed a sliding mode controller based on PID reaching law for variable intake guide vane turboshaft engines. Simulation results validated the effect of the proposed turboshaft engine modeling method and controller design method. Huang et al. [22] studied the effect of guide vane structure on the performance of tubular pump units. They analyzed the relationship between flow rate and head, power and efficiency of tubular pump units under different guide vanes. At the same time, the influence of guide vane on the Fluid mechanics performance of tubular pump was also studied. Peng et al. [23] studied a typical case study based on low head tubular units in the lower reaches of the Yellow River. According to the efficiency of the low-head tubular turbine and the hydraulic loss theory, and according to the real machine guide vane and the surface shape of turbine vane, when a fixed vane turning, they changed the guide vane outlet angle and calculated the computing velocity and energy characteristics. Alam et al. [24] conducted experimental research on the performance characteristics of Wells turbines with guide vanes in stable flow through model experiments. Then, a quasi-steady numerical analysis was performed to estimate the effect of guide vanes on the mean efficiency of the twin turbine system in unsteady flows.

At present, variable geometry turbines are still a new research direction. There is broad research space. It is not easy to achieve variable cycle functions for variable geometry turbines. Because the turbine structure is located behind the combustion chamber, the working environment of turbine guide vanes is very harsh. The guide vanes are subjected to long-term impact from high-temperature and high-pressure gas. There are few studies on the influence factors of guide vanes torque. The research of this paper fills this gap.

The torque of the guide vane is mainly determined by the pressure distribution on the pressure surface and suction surface of the guide vane. The flow rate ratio of cold and hot air flow inside and outside the guide vane has a significant impact on the pressure distribution on the surface of the guide vane. It directly affects the distribution of guide vane torque. The distribution position of gas film holes on the surface of the guide vane directly affects the pressure distribution on the guide vane surface. It has a significant impact on the distribution of guide vane torque. At the same time, cold air flow and hot air flow collide and mix in complex flow channels. This will generate a certain amount of turbulence. The turbulence also directly affects the pressure distribution on the surface of the guide vane. It also has an impact on

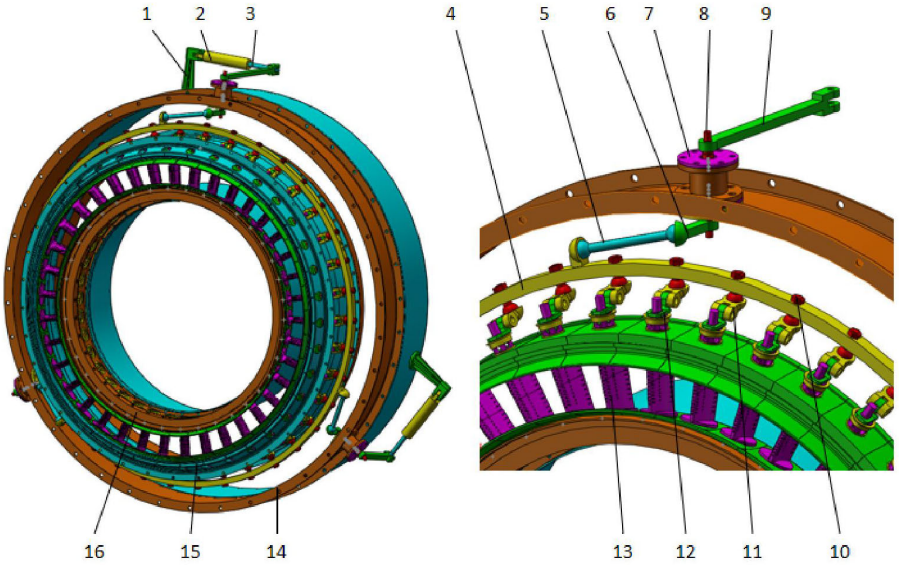

1-Base, 2-Hydraulic cylinder, 3-Piston rod, 4-Linkage ring, 5-Pull rod, 6-Paddle, 7-Bearing block, 8-Shaft, 9-Guide rod, 10-Pin, 11-Arm I, 12-Arm II, 13-Guide vane, 14-Outer casing, 15-Inner casing, 16-Inner support ring.

FIGURE 3. Three-dimensional model of three drivers' adjusting mechanism with paddle rod.

the distribution of guide vane torque. Therefore, the article mainly studies three influencing factors: turbulence intensity, flow ratio of cold and hot gas, and position distribution of gas film holes on guide vanes.

The main objective of this paper is to study three factors influencing the guide vane torque. The three influencing factors are the turbulence intensity of the gas, the flow ratio of cold gas to hot gas and the location distribution of the gas film holes on the guide vane. The main research focuses on the rule of torque of the guide vane shaft with the deflection angle at three influencing factors.

II. CFD ANALYSIS

A. COMPUTATIONAL MODEL

The main research in this paper is the torque on the guide vane shaft in the adjusting mechanism. The torque on the guide vane shaft is influenced by three factors: turbulence intensity, flow ratio, and air film hole distribution. The load on the guide vane mainly comes from two aspects. The first is the aerodynamic torque of the gas in the main channel and the cooling air flow inside the guide vane. The second is the friction torque on the shaft of the guide vane. When the guide vane rotates, the deflection angle of the guide vane is different, and the aerodynamic torque and friction torque are also different. It is necessary to study the variation law of the aerodynamic torque and the friction torque with the deflection angle at three influencing factors. Figure 3 shows the three-dimensional model of the three drivers' adjusting mechanism with paddle rod. In the calculations of this paper a partial fluid domain with circulating boundaries will be used instead of the full loop domain. Figure 4 shows the computational model of the numerical simulation. The gas and cold air inlet and outlet and circulation boundaries are also given in Figure 4.

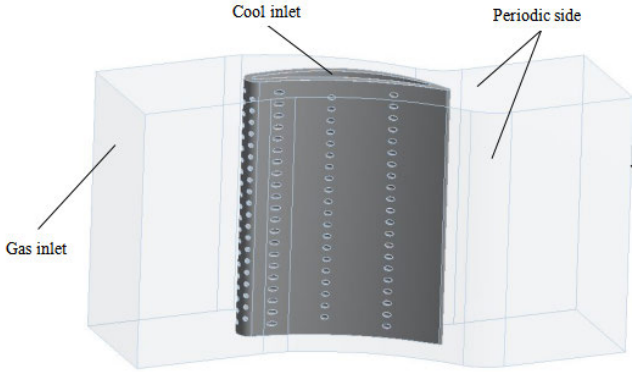

FIGURE 4. Numerical simulation calculation model.

B. CALCULATION SETTINGS

The aerodynamic torque and friction torque of the adjustable guide vane are calculated under different deflection angles. It needs to change the deflection angle of the guide vane. Figure 5 shows the change of the deflection angle of the adjustable guide vane. It can be clearly seen from Figure 5 that the position change of the guide vane during its rotation around the center of the rotating shaft. When the deflection angle is positive, the adjustable guide vane rotates counterclockwise around the rotating shaft. The opening of the guide vane increases and the flow channel becomes wider. When the deflection angle is negative, the adjustable guide vane rotates clockwise around the rotating shaft. The opening of the guide vane decreases, and the flow channel becomes

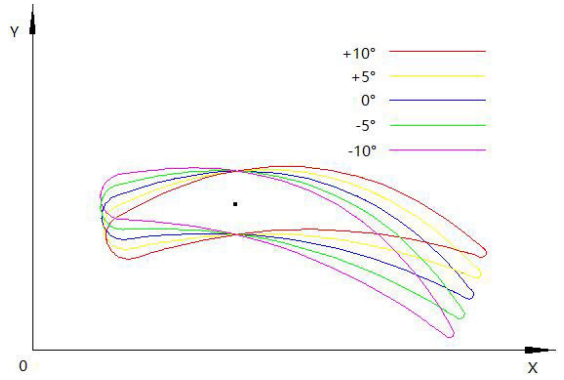

FIGURE 5. Deflection angle of adjustable guide vane.

narrower. In this paper, 11 cases of the deflection angle of the guide vane are calculated, as follows: +10°, +8°, +6°, +4°, +2°, 0°, −2°, −4°, −6°, −8°, −10°. The effects of three factors, namely, turbulence intensity, flow ratio and air film hole distribution, on the guide vane torque are also analyzed. Figure 6 shows the distribution of four different air film holes. They are no-air film hole at the leading edge (case I), no-air film hole at the trailing edge (case II), full-air film hole in the vane body (case III), and no-air film hole in the vane body (case IV).

Figure 5 shows the deflection angle of adjustable guide vane. The direction perpendicular to the tangent line of the guide vane leading edge is set as the deflection angle of 0°. The direction of rotation for increasing the throat area of the guide vane is defined as the positive direction (counter-clockwise direction). It is shown as +5° and +10° in Figure 5. The direction of rotation for reducing the throat area of the guide vane is defined as the negative direction (clockwise direction). It is shown as −5° and −10° in Figure 5. The article calculates 11 cases of +10°, +8°, +6°, +4°, +2°, 0°, −2°, −4°, −6°, −8°, −10°.

C. MESHING

Computational domain meshing is the key to numerical simulation. Figure 7 shows the calculation model grid. The quality of mesh directly affects the accuracy of numerical results. It also directly affects the convergence of the calculation results. Therefore, reasonable selection of mesh type and maximum improvement of mesh quality are very important to achieve high-precision numerical simulation [25], [26].

In this paper, the special pre-processing software GAMBIT of FLUENT is used for mesh generation. It can quickly generate high-quality unstructured meshes. It has certain advantages in dealing with complex geometric models. The main criterion of mesh quality is mesh distortion. The mesh distortion is smaller, and the quality of the generated mesh is higher. Generally speaking, regular objects can be divided into tetrahedral meshes. Its distortion will be relatively smaller.

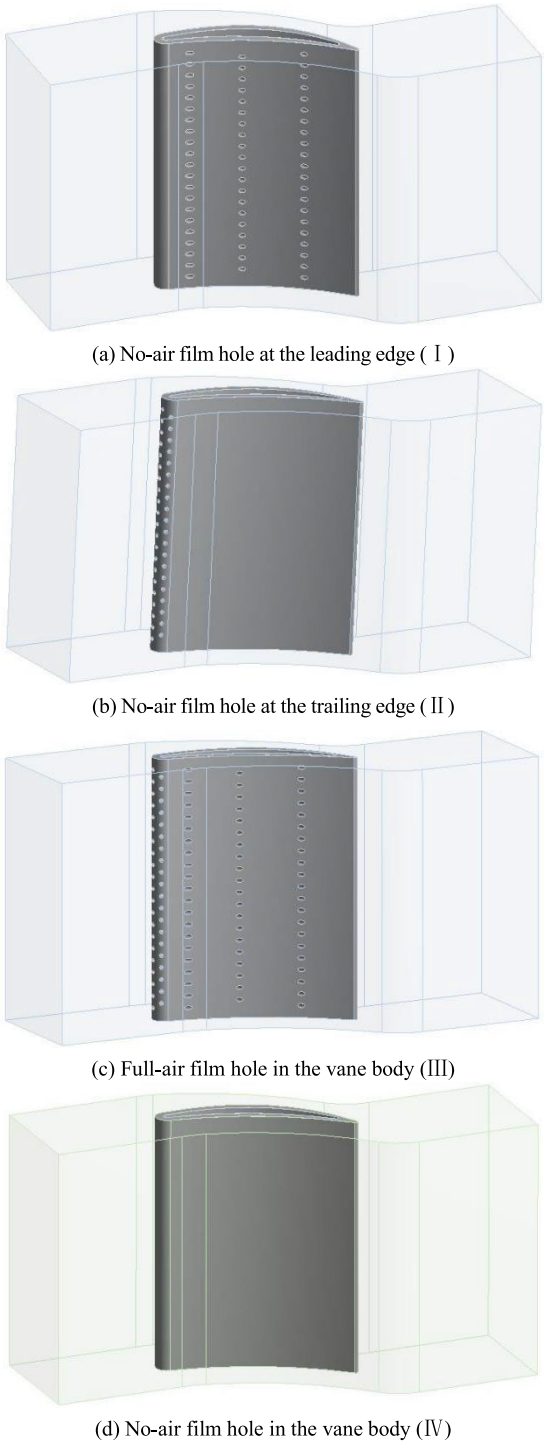

(a) No-air film hole at the leading edge (Ⅰ)

(b) No-air film hole at the trailing edge (Ⅱ)

(c) Full-air film hole in the vane body (Ⅲ)

(d) No-air film hole in the vane body (Ⅳ)

FIGURE 6. Four cases of different air film hole distributions.

D. CALCULATION METHOD AND BOUNDARY CONDITION SETTING

The research in this paper relies on the cooperation project between National Key Aero-engine Research Institute and Northeastern University. The project number is 2018JX03H002. The boundary conditions are provided by the experimental data of the institute. At the inlet boundary,

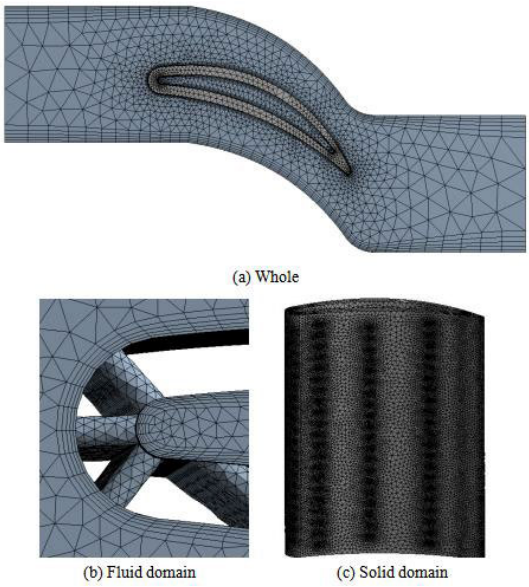

FIGURE 7. Computational model meshing.

it gives total pressure, total temperature, air flow angle, inlet turbulence and eddy viscosity ratio. It gives static pressure at the outlet boundary. The wall surface of wheel hub and rim is insulated and free of sliding. The grid pitch direction is a periodic boundary [27]. Table 1 shows the calculation method and boundary condition settings.

TABLE 1. The computation method and boundary conditions setting.

Parameter item	setting
Computation domain	Entire fluid domain
Fluid type	Compressible gas
Turbulence model	k - ε
Mainstream pressure inlet	657545.5 Pa, 1254.6 K
Cold air mass flow inlet	0.0002 kg/s, 540.8 K
Pressure outlet	264635.5 Pa
Cascade sides	Periodic boundary
Other walls	No slip adiabatic wall

III. RESULTS AND DISCUSSIONS

A. ANALYSIS OF DIFFERENT TURBULENCE INTENSITIES

1) ANALYSIS OF TEMPERATURE FIELD WITH DIFFERENT TURBULENCE INTENSITIES

The temperature load distribution on the surface of the guide vanes at different turbulence intensities and different guide vane deflection angles is given in Figure 8. It can be seen from the figure that the temperature distribution of the pressure and suction surfaces of the guide vanes clearly shows a gradient distribution change. And the surface of the guide vanes is well cooled by the air film. The cooling effect is especially significant at the position of the blade body and the trailing edge of the blade of the guide vanes. The temperature is slightly higher at the leading edge of the guide vane near the top and root of the blade. At 1% turbulence intensity, the maximum temperatures of the guide vane are 889.8K, 901.9K and 870K for the deflection angles of $+10°$, $0°$ and $-10°$, respectively. At 5% turbulence intensity, the maximum temperatures of the guide vane are 893.1K, 906K and 868.9K for the deflection angles of $+10°$, $0°$ and $-10°$, respectively. At 10% turbulence intensity, the maximum temperatures of the guide vane are 897.2K, 916.8K and 869.6K for the deflection angles of $+10°$, $0°$ and $-10°$, respectively. However, the tolerance temperature of the blade material was not exceeded. This is also more in line with the actual situation. There is an impact of mainstream hot gas at the leading edge of the blade. The cooling airflow from the air film holes is obstructed to some extent. So the cooling effect of the air film at the leading edge of the blade is slightly worse. The temperature will be slightly higher. In actual work, due to the use of over temperature, guide blade ablation phenomenon occurs more in the blade of the leading edge and trailing edge. It shows that the coupling calculation results of this paper can reflect the actual working condition of the blade more accurately.

2) ANALYSIS OF PRESSURE FIELD WITH DIFFERENT TURBULENCE INTENSITIES

The pressure load distribution on the surface of the guide vanes at different turbulence intensities and different guide vane deflection angles is given in Figure 9. It can be seen from the figure that the pressure distribution on the pressure and suction surfaces of the guide vanes clearly shows a gradient distribution change. At 1% turbulence intensity, the maximum pressures of the guide vane are 6.616×10^5Pa, 6.611×10^5Pa and 6.578×10^5Pa for the deflection angles of $+10°$, $0°$ and $-10°$, respectively. At 5% turbulence intensity, the maximum pressures of the guide vane are 6.616×10^5Pa, 6.612×10^5Pa and 6.578×10^5Pa for the deflection angles of $+10°$, $0°$ and $-10°$, respectively. At 10% turbulence intensity, the maximum pressures of the guide vane are 6.616×10^5Pa, 6.611×10^5Pa and 6.577×10^5Pa for the deflection angles of $+10°$, $0°$ and $-10°$, respectively. A distinct low-pressure area appears after each air-exhaust film holes. This is due to the cold air being ejected from the air film holes, causing the mainstream hot air in front of the air film holes to first decelerate and then accelerate. This leads to oscillations in the pressure in front of and behind the air film holes. The figure clearly shows that the pressure on the pressure surface corresponding to the leading and trailing edges of the blade is significantly higher than the pressure on the suction surface, with the rotary axis of the guide blade as the divider. This also provides data support for calculating the aerodynamic and friction torques of the guide vanes.

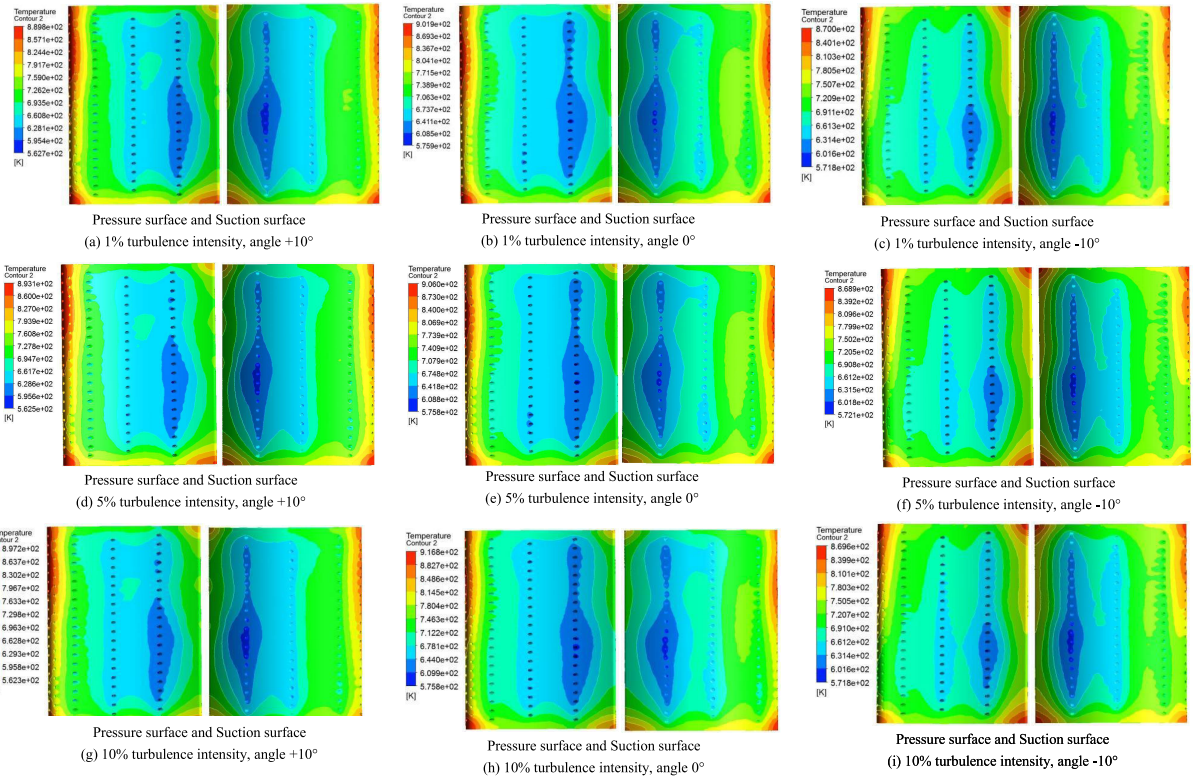

Pressure surface and Suction surface
(a) 1% turbulence intensity, angle +10°

Pressure surface and Suction surface
(b) 1% turbulence intensity, angle 0°

Pressure surface and Suction surface
(c) 1% turbulence intensity, angle -10°

Pressure surface and Suction surface
(d) 5% turbulence intensity, angle +10°

Pressure surface and Suction surface
(e) 5% turbulence intensity, angle 0°

Pressure surface and Suction surface
(f) 5% turbulence intensity, angle -10°

Pressure surface and Suction surface
(g) 10% turbulence intensity, angle +10°

Pressure surface and Suction surface
(h) 10% turbulence intensity, angle 0°

Pressure surface and Suction surface
(i) 10% turbulence intensity, angle -10°

FIGURE 8. Temperature field distribution of different turbulence intensities.

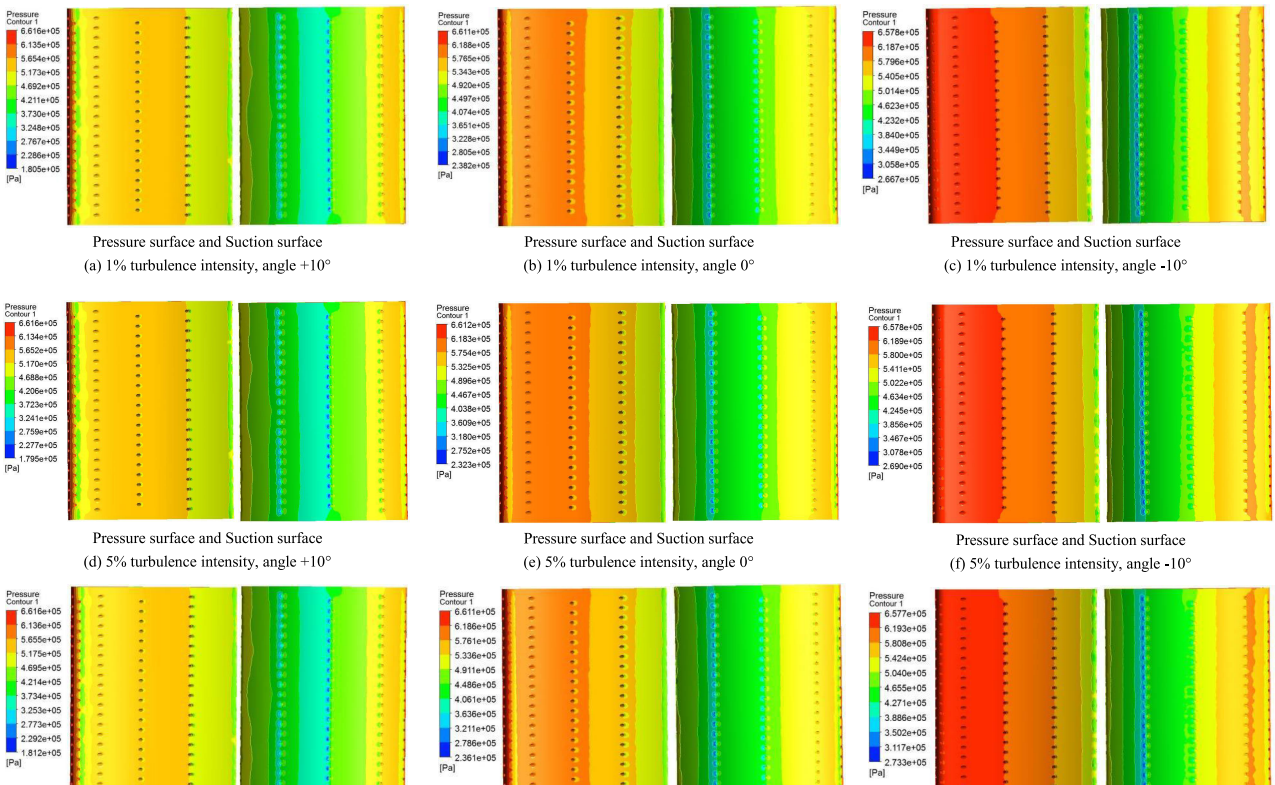

Pressure surface and Suction surface
(a) 1% turbulence intensity, angle +10°

Pressure surface and Suction surface
(b) 1% turbulence intensity, angle 0°

Pressure surface and Suction surface
(c) 1% turbulence intensity, angle -10°

Pressure surface and Suction surface
(d) 5% turbulence intensity, angle +10°

Pressure surface and Suction surface
(e) 5% turbulence intensity, angle 0°

Pressure surface and Suction surface
(f) 5% turbulence intensity, angle -10°

Pressure surface and Suction surface
(g) 10% turbulence intensity, angle +10°

Pressure surface and Suction surface
(h) 10% turbulence intensity, angle 0°

Pressure surface and Suction surface
(i) 10% turbulence intensity, angle -10°

FIGURE 9. Pressure field distribution of different turbulence intensities.

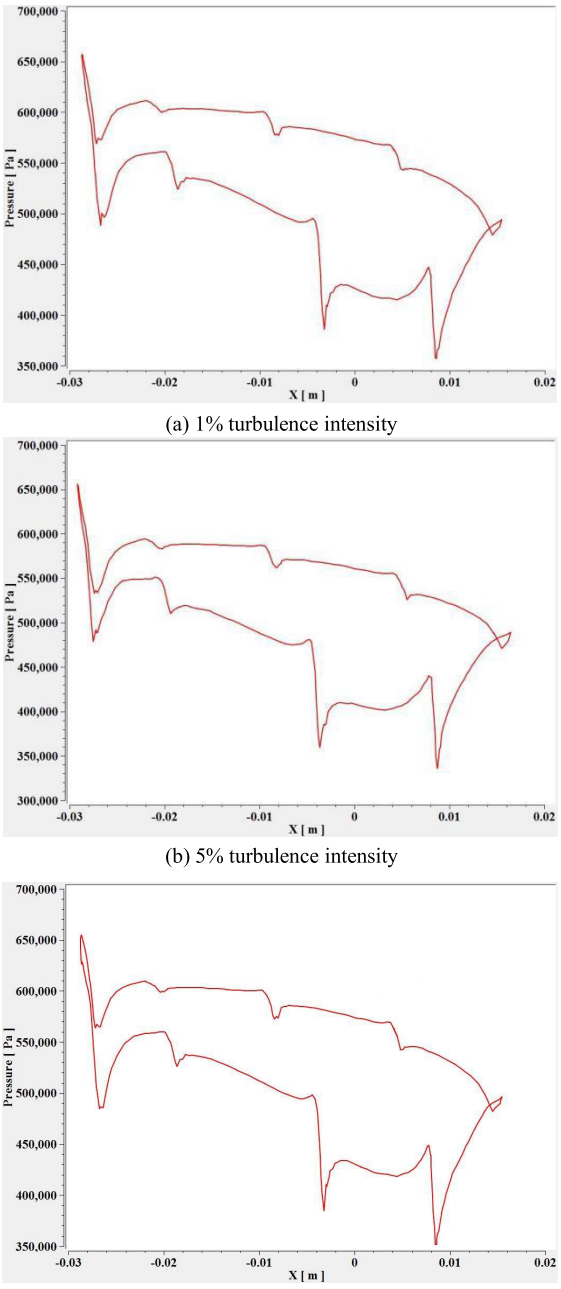

(a) 1% turbulence intensity

(b) 5% turbulence intensity

(c) 10% turbulence intensity

FIGURE 10. Pressure distribution at 50% blade height of different turbulence intensities.

3) PRESSURE ANALYSIS AT 50% BLADE HEIGHT FOR DIFFERENT TURBULENCE INTENSITIES

Figure 10 shows the cross-sectional pressure distribution at 50% blade height of the guide vane at different turbulence intensities. It can be seen from the figure that at 1% turbulence intensity, 5% turbulence intensity, and 10% turbulence intensity, low pressure areas appear near each exhaust film holes of the guide vane. That is, a sudden drop in pressure. This is due to the cold air being ejected from the air film holes, causing the mainstream hot air in front of the air film holes to first decelerate and then accelerate. This leads to oscillations in the pressure in front of and behind the air film holes. In addition, the pressure on the pressure side of the guide vane is always higher than the pressure on the suction side. This causes the guide vanes to be subjected to high lateral pressure. It generates aerodynamic and friction torque at the shaft of the guide vane.

B. ANALYSIS OF DIFFERENT FLOW RATIOS

1) ANALYSIS OF TEMPERATURE FIELD WITH DIFFERENT FLOW RATIOS

Figure 11 shows the temperature load distribution on the surface of the guide vanes at different flow ratios and different guide vane deflection angles. It can be seen from the figure that the temperature distribution of the pressure and suction surfaces of the guide vanes clearly shows a gradient distribution change. And the surface of the guide vanes is well cooled by the air film. The cooling effect is especially significant at the position of the blade body and the trailing edge of the blade of the guide vanes. The temperature is slightly higher at the leading edge of the guide vane near the top and root of the blade. At 4% flow ratio, the maximum temperatures of the guide vane are 893.1K, 906K and 868.9K for the deflection angles of $+10°$, $0°$ and $-10°$, respectively. At 8% flow ratio, the maximum temperatures of the guide vane are 849.7K, 860.8K and 842K for the deflection angles of $+10°$, $0°$ and $-10°$, respectively. At 12% flow ratio, the maximum temperatures of the guide vane are 842.9K, 841.6K and 834.2K for the deflection angles of $+10°$, $0°$ and $-10°$, respectively. However, the tolerance temperature of the blade material was not exceeded. This is also more in line with the actual situation. At the leading edge of the blade the cooling airflow from the air film holes is obstructed to some extent due to the impact of the mainstream hot gas. So the cooling effect of the air film at the leading edge of the blade is slightly worse. The temperature will be slightly higher. In actual work, due to the use of over temperature, guide blade ablation phenomenon occurs more in the blade of the leading edge and trailing edge. It shows that the coupling calculation results of this paper can reflect the actual working condition of the blade more accurately.

2) ANALYSIS OF PRESSURE FIELD WITH DIFFERENT FLOW RATIOS

The pressure load distribution on the surface of the guide vanes at different flow ratios and different guide vane deflection angles is given in Figure 12. It can be seen from the figure that the pressure distribution on the pressure and suction surfaces of the guide vanes clearly shows a gradient distribution change. At 4% flow ratio, the maximum pressures of the guide vane are 7.581×10^5Pa, 7.588×10^5Pa and 7.578×10^5Pa for the deflection angles of $+10°$, $0°$ and $-10°$, respectively. At 8% flow ratio, the maximum pressures of the guide vane are 7.083×10^5Pa, 7.084×10^5Pa and 7.074×10^5Pa for the deflection angles of $+10°$, $0°$ and

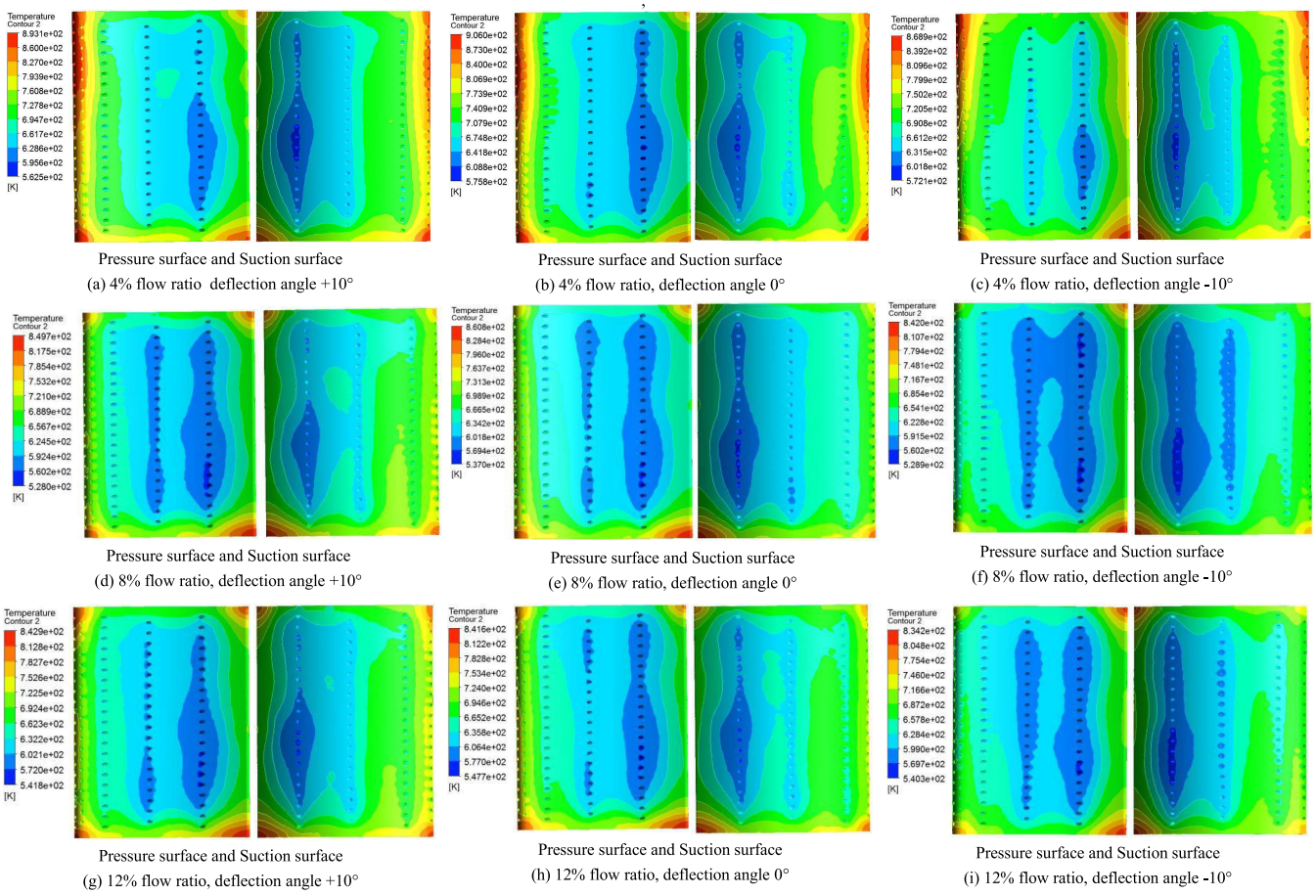

FIGURE 11. Temperature field distribution of different flow ratios.

-10°, respectively. At 12% flow ratio, the maximum pressures of the guide vane are 6.615×10^5Pa, 6.612×10^5Pa and 6.578×10^5Pa for the deflection angles of +10°, 0° and -10°, respectively. A distinct low-pressure area appears after each air-exhaust film holes. This is due to the cold air being ejected from the air film holes, causing the mainstream hot air in front of the air film holes to first decelerate and then accelerate. This leads to oscillations in the pressure in front of and behind the air film holes. The figure clearly shows that the pressure on the pressure surface corresponding to the leading and trailing edges of the blade is significantly higher than the pressure on the suction surface, with the rotary axis of the guide blade as the divider. This also provides data support for calculating the aerodynamic and friction torques of the guide vanes.

3) PRESSURE ANALYSIS AT 50% BLADE HEIGHT FOR DIFFERENT FLOW RATIOS

Figure 13 shows the cross-sectional pressure distribution at 50% blade height of the guide vane at different flow ratios. It can be seen from the figure that at 4% flow ratio, 8% flow ratio, and 12% flow ratio, low pressure areas appear near each exhaust film holes of the guide vane. That is, a sudden drop in pressure. This is due to the cold air being ejected from the air film holes, causing the mainstream hot air in front of the air film holes to first decelerate and then accelerate. This leads to oscillations in the pressure in front of and behind the air film holes. In addition, the pressure on the pressure side of the guide vane is always higher than the pressure on the suction side. This causes the guide vanes to be subjected to high lateral pressure. It generates aerodynamic and friction torque at the shaft of the guide vane.

C. ANALYSIS OF DIFFERENT AIR FILM HOLE DISTRIBUTIONS

1) ANALYSIS OF TEMPERATURE FIELD WITH DIFFERENT AIR FILM HOLE DISTRIBUTIONS

The temperature load distribution on the surface of the guide vanes at 4 different air film hole distributions is given in Figure 14. The four distributions are no-air film hole at the leading edge (case I), no-air film hole at the trailing edge (case II), full-air film hole in the vane body (case III) and no-air film hole in the vane body (case IV) respectively. It can be seen from the figure that the temperature distribution of the pressure and suction surfaces of the guide vanes clearly shows a gradient distribution change. At 4 different air film

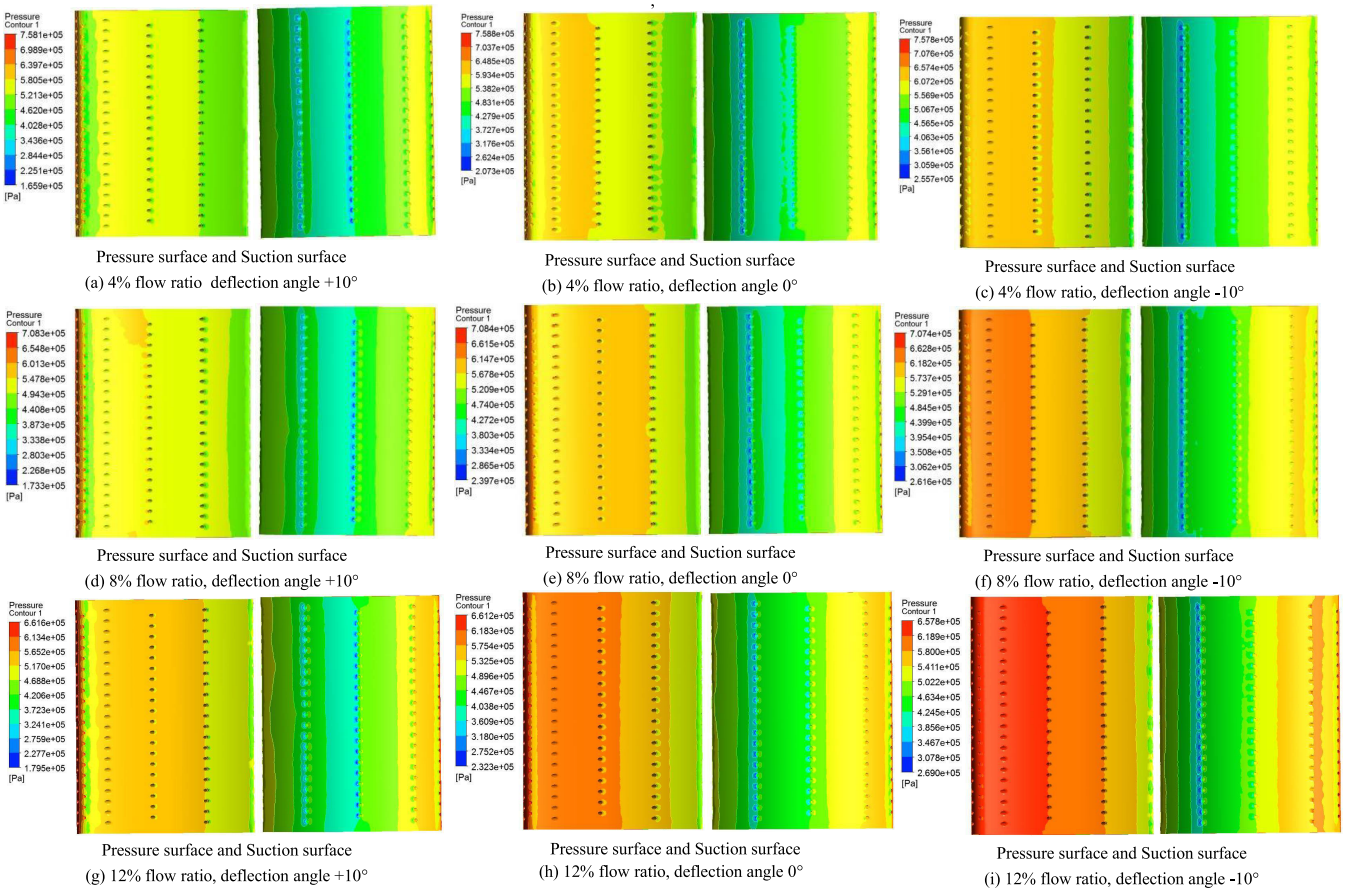

FIGURE 12. **Pressure field distribution of different flow ratios.**

hole distributions of case I, case II, case III and case IV, the maximum temperatures of the guide vane are 919.5K, 1004K, 906K and 994.3K respectively. However, the tolerance temperature of the blade material was not exceeded. This is also more in line with the actual situation. In actual work, due to the use of over temperature, guide blade ablation phenomenon occurs more in the blade of the leading edge and trailing edge. It shows that the coupling calculation results of this paper can reflect the actual working condition of the blade more accurately.

2) ANALYSIS OF PRESSURE FIELD WITH DIFFERENT AIR FILM HOLE DISTRIBUTIONS

The pressure load distribution on the surface of the guide vanes at 4 different air film hole distributions is given in Figure 15. The four distributions are no-air film hole at the leading edge (case I), no-air film hole at the trailing edge (case II), full-air film hole in the vane body (case III) and no-air film hole in the vane body (case IV) respectively. It can be seen from the figure that the pressure distribution on the pressure and suction surfaces of the guide vanes clearly shows a gradient distribution change. At 4 different air film hole distributions of case I, case II, case III and case IV, the maximum pressures of the guide vane are 7.108×10^5Pa, 7.096×10^5Pa, 6.612×10^5Pa and 6.572×10^5Pa respectively. A distinct low-pressure area appears after each air-exhaust film holes. This is due to the cold air being ejected from the air film holes, causing the mainstream hot air in front of the air film holes to first decelerate and then accelerate. This leads to oscillations in the pressure in front of and behind the air film holes. The figure clearly shows that the pressure on the pressure surface corresponding to the leading and trailing edges of the blade is significantly higher than the pressure on the suction surface, with the rotary axis of the guide blade as the divider. This also provides data support for calculating the aerodynamic and friction torques of the guide vanes.

3) PRESSURE ANALYSIS AT 50% BLADE HEIGHT FOR DIFFERENT AIR FILM HOLE DISTRIBUTIONS

Figure 16 shows the cross-sectional pressure distribution at 50% blade height of the guide vane at 4 different air film hole distributions. The four distributions are no-air film hole at the leading edge (case I), no-air film hole at the trailing edge (case II), full-air film hole in the vane body (case III) and no-air film hole in the vane body (case IV) respectively. It can be seen from the figure that at 4 different air film hole distributions of case I, case II, case III and case IV, low

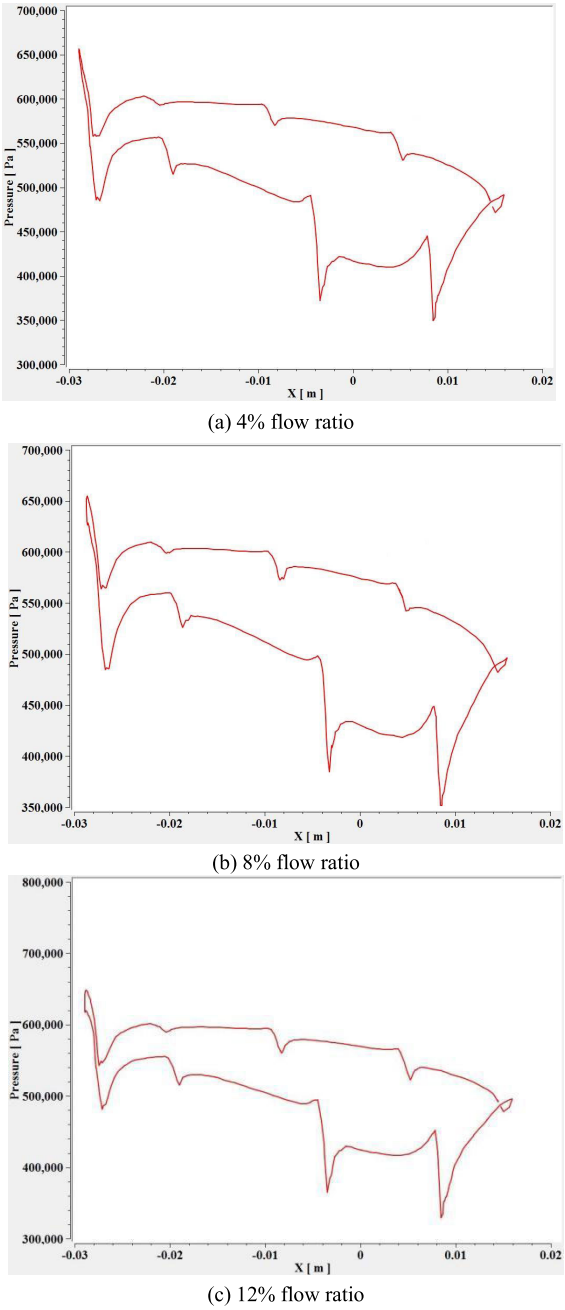

(a) 4% flow ratio

(b) 8% flow ratio

(c) 12% flow ratio

FIGURE 13. Pressure distribution at 50% blade height of different flow ratios.

pressure areas appear near each exhaust film holes of the guide vane. That is, a sudden drop in pressure. This is due to the cold air being ejected from the air film holes, causing the mainstream hot air in front of the air film holes to first decelerate and then accelerate. This leads to oscillations in the pressure in front of and behind the air film holes. In addition, the pressure on the pressure side of the guide vane is always higher than the pressure on the suction side. This causes the guide vanes to be subjected to high lateral pressure. It generates aerodynamic and friction torque at the shaft of the guide vane.

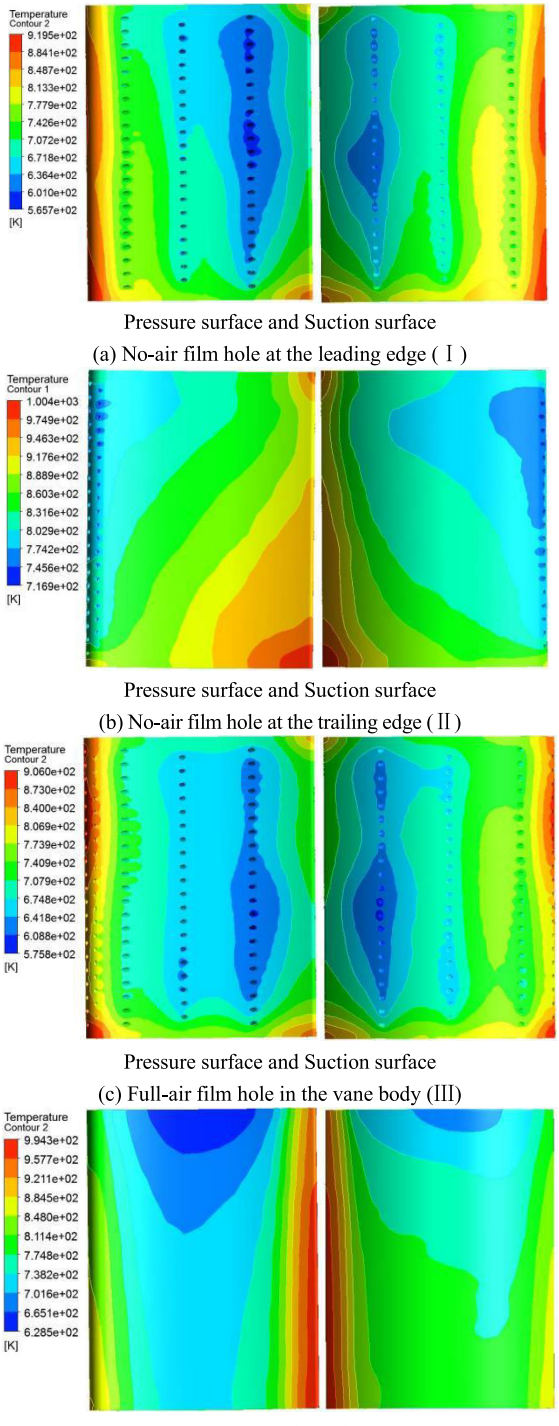

Pressure surface and Suction surface

(a) No-air film hole at the leading edge (Ⅰ)

Pressure surface and Suction surface

(b) No-air film hole at the trailing edge (Ⅱ)

Pressure surface and Suction surface

(c) Full-air film hole in the vane body (Ⅲ)

Pressure surface and Suction surface

(d) No-air film hole in the vane body (Ⅳ)

FIGURE 14. Temperature field distribution of different air film hole distributions.

D. VELOCITY FIELD ANALYSIS

Figure 17 shows the velocity distribution of the air flow in the inner channel for the deflection angles of the guide vane of $+10°$, $0°$ and $-10°$ respectively. Gas flows outside the guide vanes. Cold air flows inside the guide vanes. It can be seen from the figure that the velocity of the air flow

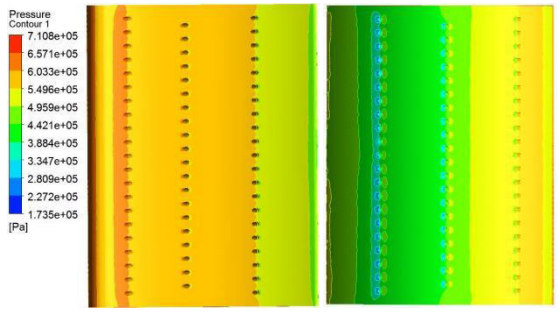

Pressure surface and Suction surface

(a) No-air film hole at the leading edge (Ⅰ)

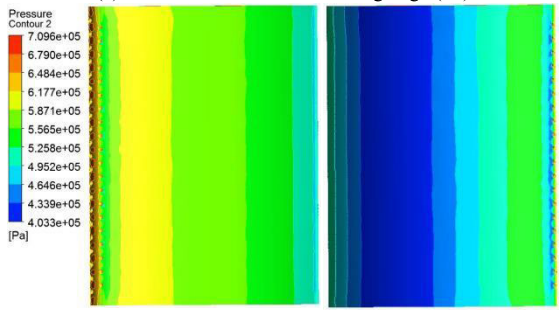

Pressure surface and Suction surface

(b) No-air film hole at the trailing edge (Ⅱ)

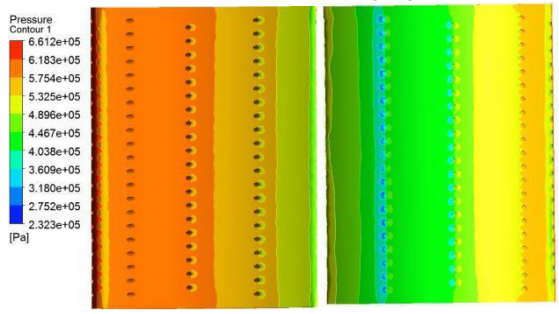

Pressure surface and Suction surface

(c) Full-air film hole in the vane body (Ⅲ)

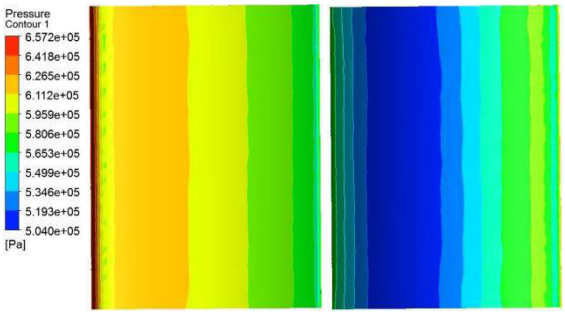

Pressure surface and Suction surface

(d) No-air film hole in the vane body (Ⅳ)

FIGURE 15. Pressure field distribution of different air film hole distributions.

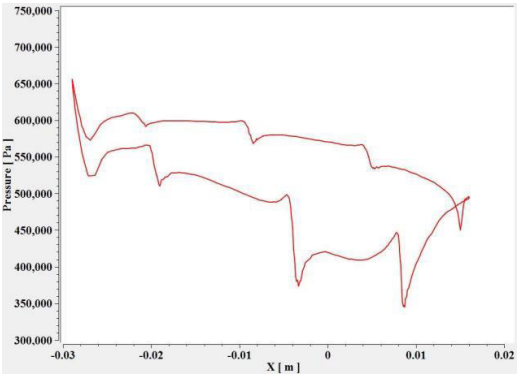

(a) No-air film hole at the leading edge (Ⅰ)

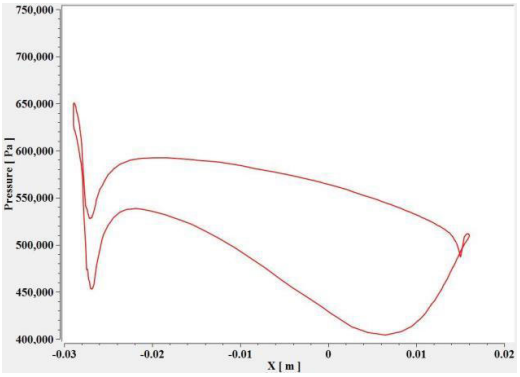

(b) No-air film hole at the trailing edge (Ⅱ)

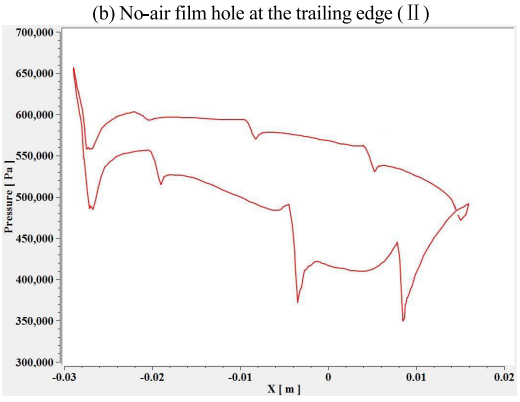

(c) Full-air film hole in the vane body (Ⅲ)

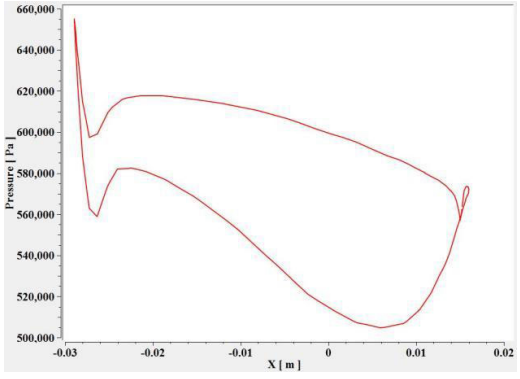

(d) No-air film hole in the vane body (Ⅳ)

FIGURE 16. Pressure distribution at 50% blade height of different air film hole distributions.

clearly shows a gradient distribution. The velocity of gas flow gradually increases from the inlet. The velocity reaches a maximum near the guide vane trailing edge. The maximums of the speed are 600.8m/s, 534.4m/s and 522.5m/s for the deflection angles of $+10°$, $0°$ and $-10°$, respectively. From the velocity distribution of the cold air in the guide vane, it can be seen that the cold air in the guide vane is

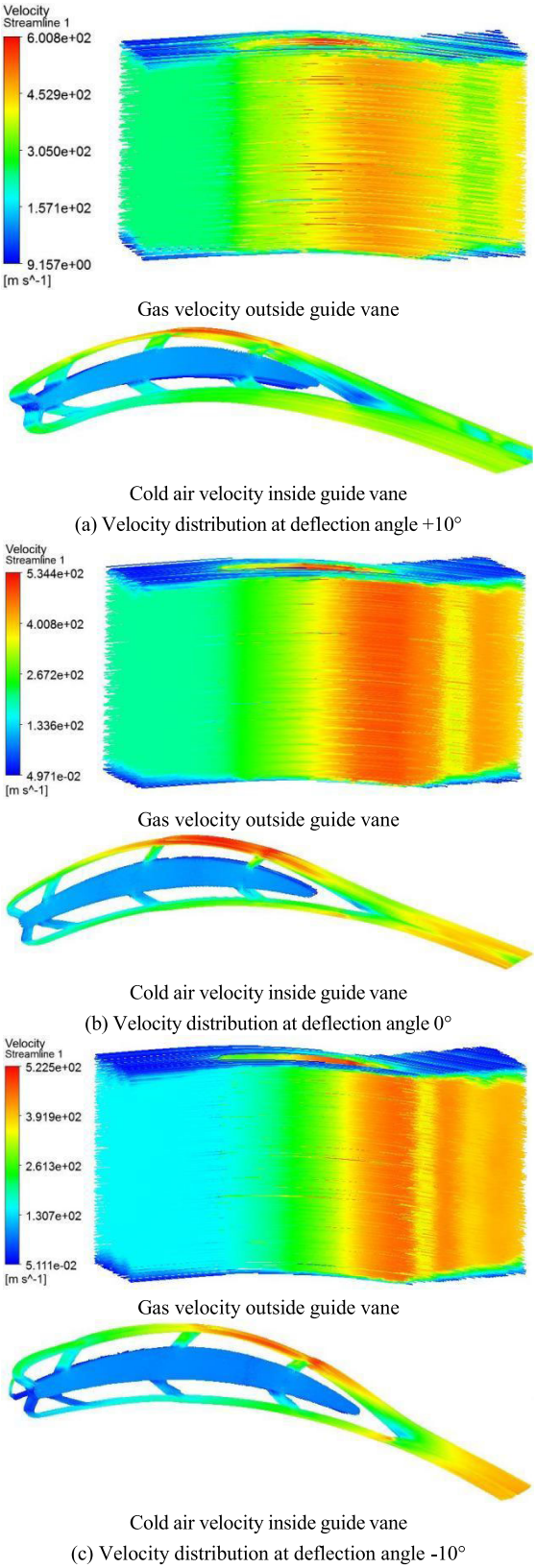

FIGURE 17. Velocity field distribution at different deflection angles.

ejected from the film hole. The cold air is impacted by the high-speed gas outside the guide vane. The cold air flows completely against the outer surface of the guide vanes. The velocity of cold air also presents a gradient distribution. The speed reaches the maximum near the trailing edge of the guide vane. Table 2 shows the maximum velocities of the flow field at different deflection angles. Figure 18 shows that the maximum velocity of the flow field increases with increasing deflection angle. From Table 2 and Figure 18, it can be seen that the maximum velocities of the flow field are 522.5m/s, 523.1m/s, 523.5m/s, 525.7m/s, 528.6m/s, 534.4m/s, 534.8m/s, 542.2m/s, 553.4m/s, 573.2m/s and 600.8m/s for the guide vane deflection angles of $-10°$, $-8°$, $-6°$, $-4°$, $-2°$, $0°$, $+2°$, $+4°$, $+6°$, $+8°$ and $+10°$, respectively.

E. GRID INDEPENDENCE VERIFICATION

Table 3 shows the resultant torque of different grid quantities. Figure 19 shows the influence of grid quantity on the resultant torque of guide vane at deflection angle. The article presents the effects of different grid quantities on the resultant torque. From Table 3 and Figure 19, it can be seen that at grid quantities of 3.41 million, 4.33 million, 5.16 million and 5.85 million, the resultant torque of the guide vane first increases and then decreases with the deflection angle. At the deflection angle $-2°$, the resultant torque reaches the maximum value. The resultant torques are 3.631239N·m, 3.641224N·m, 3.654639N·m and 3.66782N·m for grid quantities of 3.41 million, 4.33 million, 5.16 million and 5.85 million, respectively. At the deflection angle $+10°$, the resultant torque reaches the minimum value. The resultant torques are 2.996647N·m, 2.912139N·m, 2.806459N·m and 2.823353N·m for grid quantities of 3.41 million, 4.33 million, 5.16 million and 5.85 million, respectively. As the number of grids increases, the resultant torque of the guide vane tends to stabilize. When the number of grids increases from 5.16 million to 5.85 million, the resultant torque of the guide vane basically does not change. Therefore, the article selects the grid quantity of 5.85 million for numerical calculation.

F. ANALYSIS OF AERODYNAMIC TORQUE AND FRICTION TORQUE WITH UNSTEADY EFFECTS

Table 4 shows the aerodynamic torque of unsteady effects at deflection angles. Figure 20 shows the aerodynamic torque of guide vane with unsteady effects. From Table 4 and Figure 20, it can be seen that at the deflection angles of $-10°$, $0°$, $+10°$, the aerodynamic torque of the guide vane increases with the time step. And in the time step range of 100 to 1100, the aerodynamic torques increase to 0.847862N·m, 1.11686N·m and 0.533352N·m for the deflection angles of $-10°$, $0°$, $+10°$, respectively. However, in the time step range of 1100 to 1500, the aerodynamic torques do not change with time steps for the deflection angles of $-10°$, $0°$, $+10°$, respectively. The aerodynamic torque of the guide vane tends to stabilize. The maximum values of aerodynamic torques are 0.847974N·m, 1.11755N·m and 0.534265N·m for the deflection angles of $-10°$, $0°$, $+10°$, respectively.

TABLE 2. Maximum velocity of the flow field with different deflection angles.

	Deflection angle[°]										
	-10	-8	-6	-4	-2	0	2	4	6	8	10
Velocity [m/s]	522.5	523.1	523.5	525.7	528.6	534.4	534.8	542.2	553.4	573.2	600.8

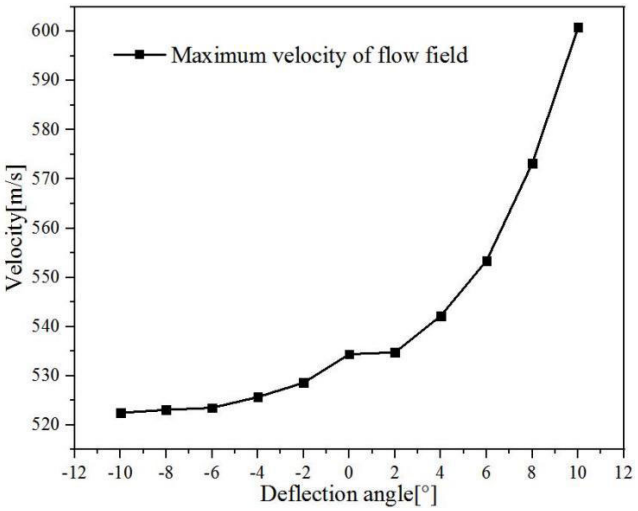

FIGURE 18. Maximum velocity of the flow field with different deflection angles.

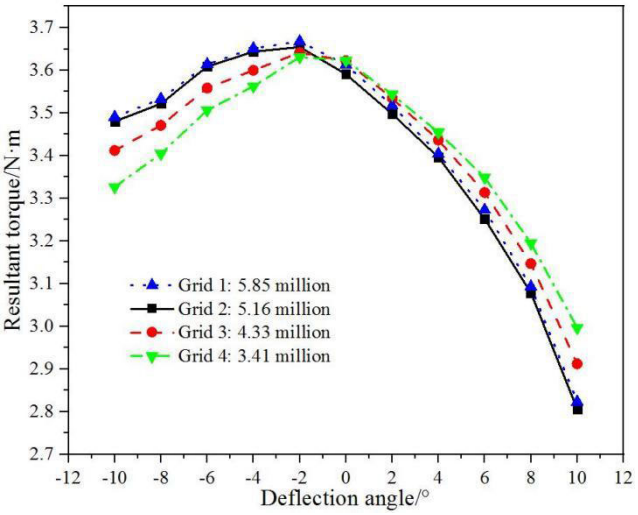

FIGURE 19. The influence of grid quantity on the resultant torque of guide vane at deflection angle.

Table 5 shows the friction torque of unsteady effects at deflection angles. Figure 21 shows the friction torque of guide vane with unsteady effects. From Table 5 and Figure 21, it can be seen that at the deflection angles of −10°, 0°, +10°, the friction torque of the guide vane increases with the time step. And in the time step range of 100 to 1100,

TABLE 3. Resultant torque of different grid quantities.

Deflection angle[°]	Resultant torque[N·m]			
	Grid 4: 3.41 million	Grid 3: 4.33 million	Grid 2: 5.16 million	Grid 1: 5.85 million
-10	3.326485	3.412246	3.480153	3.490548
-8	3.404857	3.471147	3.521768	3.533144
-6	3.506755	3.558324	3.608965	3.614163
-4	3.562468	3.600145	3.643597	3.651426
-2	3.631239	3.641224	3.654639	3.66782
0	3.623238	3.622356	3.591137	3.6127
+2	3.543654	3.534438	3.497658	3.517286
+4	3.454568	3.436558	3.396057	3.40411
+6	3.348765	3.313516	3.251647	3.272716
+8	3.194955	3.146785	3.078654	3.093202
+10	2.996647	2.912139	2.806459	2.823353

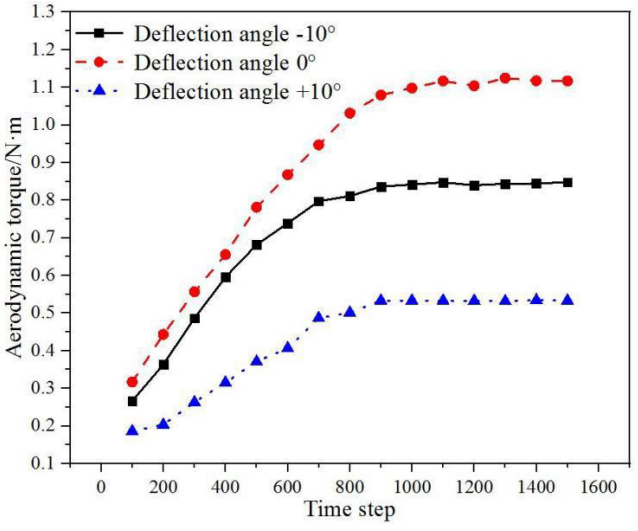

FIGURE 20. Aerodynamic torque of guide vane with unsteady effects.

the friction torques increase to 2.73134N·m, 2.61346N·m and 2.35275N·m for the deflection angles of −10°, 0°, +10°,

TABLE 4. Aerodynamic torque of unsteady effects at deflection angles.

Time step	Aerodynamic torque[N·m]		
	Deflection angle -10°	Deflection angle 0°	Deflection angle +10°
100	0.266552	0.316512	0.186062
200	0.363423	0.443372	0.203286
300	0.486467	0.556359	0.26314
400	0.59587	0.65537	0.31522
500	0.68167	0.78128	0.37098
600	0.73893	0.86767	0.40663
700	0.79744	0.94716	0.48684
800	0.811348	1.031314	0.500997
900	0.836552	1.07959	0.533432
1000	0.841952	1.09827	0.533432
1100	0.847862	1.11686	0.533352
1200	0.839765	1.10458	0.532618
1300	0.843967	1.12469	0.531947
1400	0.844586	1.11755	0.534265
1500	0.847974	1.11743	0.533186

TABLE 5. Friction torque of unsteady effects at deflection angles.

Time step	Friction torque[N·m]		
	Deflection angle -10°	Deflection angle 0°	Deflection angle +10°
100	0.55136	0.37191	0.26026
200	0.79978	0.67032	0.49863
300	1.10073	0.89246	0.68935
400	1.32633	1.10777	0.96588
500	1.52205	1.29322	1.16196
600	1.74345	1.50508	1.36253
700	1.86656	1.69724	1.53582
800	2.02647	1.90787	1.75526
900	2.26573	2.10702	1.97431
1000	2.54115	2.39312	2.20016
1100	2.73134	2.61346	2.35275
1200	2.75278	2.65389	2.38098
1300	2.74587	2.64741	2.37617
1400	2.75428	2.65826	2.38237
1500	2.75758	2.65814	2.38659

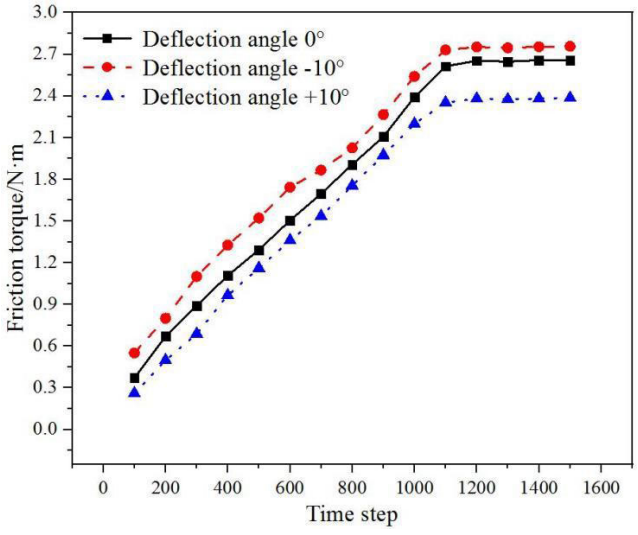

FIGURE 21. Friction torque of guide vane with unsteady effects.

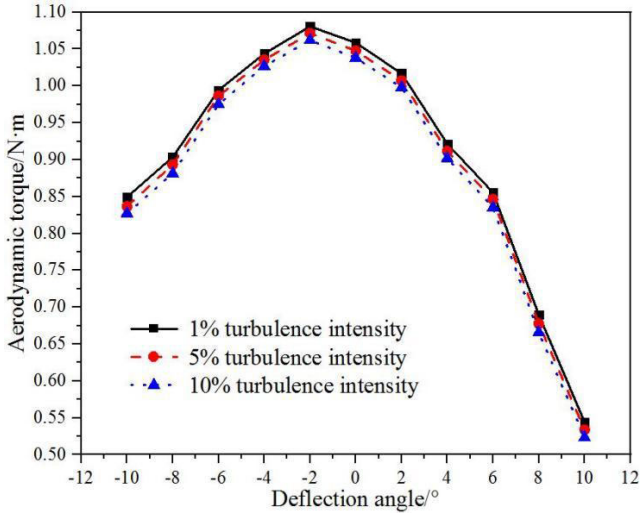

FIGURE 22. The relationship between aerodynamic torque and deflection angle at different turbulence intensities.

respectively. However, in the time step range of 1100 to 1500, the friction torques do not change with time steps for the deflection angles of −10°, 0°, +10°, respectively. The friction torque of the guide vane tends to stabilize. The maximum values of friction torques are 2.75758N·m, 2.65826N·m and 2.38659N·m for the deflection angles of −10°, 0°, +10°, respectively.

G. ANALYSIS OF AERODYNAMIC TORQUE AND FRICTION TORQUE WITH DIFFERENT TURBULENCE INTENSITIES

Combined with UDF program operation, the aerodynamic torque of the guide vane is calculated. Table 6 shows the aerodynamic torque at different turbulence intensities. Table 6 gives the aerodynamic torques of the guide vane for the

TABLE 6. Aerodynamic torque of different turbulence intensities.

Deflection angle[°]	Aerodynamic torque[N·m]		
	1% turbulence intensity	5% turbulence intensity	10% turbulence intensity
-10	0.849365	0.836501	0.827168
-8	0.903564	0.893370	0.881286
-6	0.994132	0.986357	0.975267
-4	1.04379	1.03536	1.026675
-2	1.08067	1.07129	1.06198
0	1.05863	1.04766	1.037984
+2	1.01685	1.00715	0.99786
+4	0.921348	0.911315	0.901797
+6	0.855347	0.846209	0.835219
+8	0.689743	0.677621	0.665729
+10	0.544089	0.533761	0.523507

deflection angles of −10°, −8°, −6°, −4°, −2°, 0°, +2°, +4°, +6°, +8° and +10° at 1%, 5% and 10% turbulence intensities. Figure 22 shows the relationship between aerodynamic torque and deflection angle at different turbulence intensities. From Table 6 and Figure 22, it can be seen that at 1%, 5% and 10% turbulence intensities, the aerodynamic torque of the guide vane first increases and then decreases with the deflection angle. At the deflection angle −2°, the aerodynamic torque reaches the maximum value. The aerodynamic torques are 1.08067N·m, 1.07129N·m and 1.06198N·m for the turbulence intensities of 1%, 5% and 10%, respectively. At the deflection angle +10°, the aerodynamic torque reaches the minimum value. The aerodynamic torques are 0.544089N·m, 0.533761N·m and 0.523507N·m for the turbulence intensities of 1%, 5% and 10%, respectively. And with the turbulence intensity increasing, the aerodynamic torque of the guide vane slightly decreases. At the same deflection angle, the aerodynamic torques of 1%, 5% and 10% turbulence intensities decrease sequentially.

Combined with UDF program operation, the friction torque of the guide vane is calculated. Table 7 shows the friction torque at different turbulence intensities. Table 7 gives the friction torques of the guide vane for the deflection angles of −10°, −8°, −6°, −4°, −2°, 0°, +2°, +4°, +6°, +8° and +10° at 1%, 5% and 10% turbulence intensities. Figure 23 shows the relationship between friction torque and deflection angle at different turbulence intensities. It can be seen from Table 7 and Figure 23 that at the turbulence intensities of 1%, 5% and 10%, the friction torque of the guide vane decreases with the deflection angle. At the deflection angle −10°, the friction torque reaches the maximum value. The friction torques are 2.74186N·m, 2.73135N·m and 2.72179N·m for

TABLE 7. Friction torque of different turbulence intensities.

Deflection angle[°]	Friction torque[N·m]		
	1% turbulence intensity	5% turbulence intensity	10% turbulence intensity
-10	2.74186	2.73135	2.72179
-8	2.72984	2.71979	2.70957
-6	2.72011	2.71072	2.70063
-4	2.70644	2.69631	2.68597
-2	2.68167	2.67204	2.66197
0	2.65285	2.64346	2.63416
+2	2.61548	2.60657	2.59782
+4	2.57589	2.56643	2.55684
+6	2.51465	2.50572	2.49652
+8	2.45014	2.44113	2.43234
+10	2.36145	2.35275	2.34388

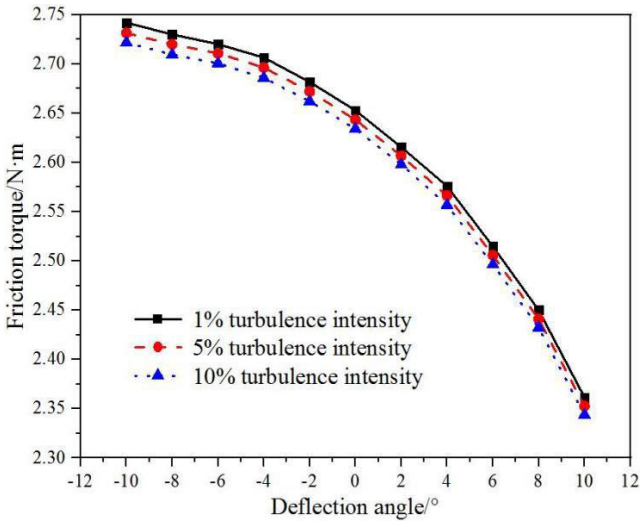

FIGURE 23. The relationship between friction torque and deflection angle at different turbulence intensities.

the turbulence intensities of 1%, 5% and 10%, respectively. At the deflection angle +10°, the friction torque reaches the minimum value. The friction torques are 2.36145N·m, 2.35275N·m and 2.34388N·m for the turbulence intensities of 1%, 5% and 10%, respectively. And with the turbulence intensity increasing, the friction torque of the guide vane slightly decreases. At the same deflection angle, the friction torques of 1%, 5% and 10% turbulence intensities decrease sequentially.

H. ANALYSIS OF AERODYNAMIC TORQUE AND FRICTION TORQUE WITH DIFFERENT FLOW RATIOS

Combined with UDF program operation, the aerodynamic torque of the guide vane is calculated. Table 8 shows the

TABLE 8. Aerodynamic torque of different flow ratios.

Deflection angle[°]	Aerodynamic torque[N·m]		
	4% flow ratio	8% flow ratio	12% flow ratio
-10	0.836552	0.783108	0.739206
-8	0.893370	0.836514	0.779425
-6	0.986314	0.929963	0.878617
-4	1.03522	0.985836	0.938162
-2	1.07167	1.02416	0.948665
0	1.04893	0.99376	0.920478
+2	1.00715	0.934746	0.879731
+4	0.911315	0.862730	0.807491
+6	0.846293	0.792776	0.738397
+8	0.677637	0.623164	0.583537
+10	0.533761	0.493313	0.441955

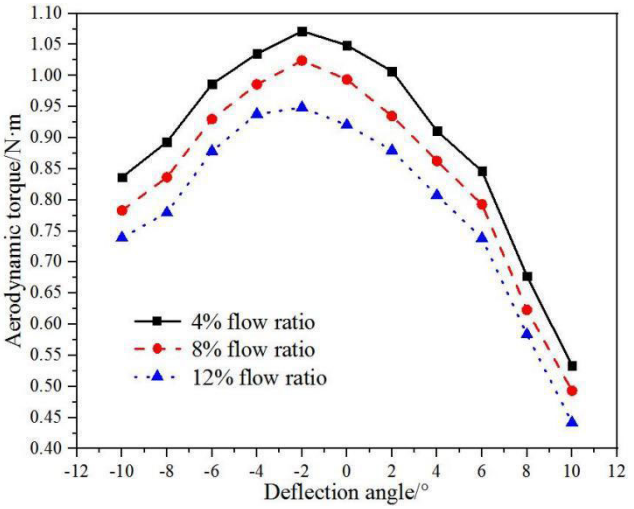

FIGURE 24. The relationship between aerodynamic torque and deflection angle at different flow ratios.

aerodynamic torque at different flow ratios. Table 8 gives the aerodynamic torques of the guide vane for the deflection angles of −10°, −8°, −6°, −4°, −2°, 0°, +2°, +4°, +6°, +8° and +10° at 4%, 8% and 12% flow ratios. Figure 24 shows the relationship between aerodynamic torque and deflection angle at different flow ratios. From Table 8 and Figure 24, it can be seen that at 4%, 8% and 12% flow ratios, the aerodynamic torque of the guide vane first increases and then decreases with the deflection angle. At the deflection angle −2°, the aerodynamic torque reaches the maximum value. The aerodynamic torques are 1.07167N·m, 1.02416N·m and 0.948665N·m for the flow ratios of 4%, 8% and 12%, respectively. At the deflection angle +10°, the aerodynamic torque reaches the minimum value. The aerodynamic torques are 0.533761N·m, 0.493313N·m and 0.441955N·m for the flow ratios of 4%, 8% and 12%, respectively. And with the flow ratio increasing, the aerodynamic torque of the guide vane slightly decreases. At the same deflection angle, the aerodynamic torques of 4%, 8% and 12% flow ratios decrease sequentially.

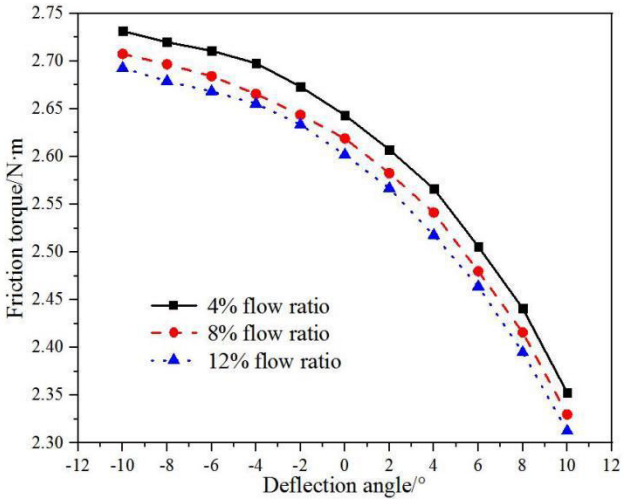

FIGURE 25. The relationship between friction torque and deflection angle at different flow ratios.

TABLE 9. Friction torque of different flow ratios.

Deflection angle[°]	Friction torque[N·m]		
	4% flow ratio	8% flow ratio	12% flow ratio
-10	2.73135	2.70744	2.69270
-8	2.71979	2.69663	2.67896
-6	2.71072	2.6842	2.66824
-4	2.69777	2.66559	2.65528
-2	2.67322	2.64366	2.63349
0	2.64346	2.61894	2.60193
+2	2.60724	2.58254	2.56671
+4	2.56643	2.54138	2.51768
+6	2.50572	2.47994	2.46403
+8	2.44113	2.41582	2.39494
+10	2.35275	2.33004	2.31268

Combined with UDF program operation, the friction torque of the guide vane is calculated. Table 9 shows the friction torque at different flow ratios. Table 9 gives the friction torques of the guide vane for the deflection angles of −10°, −8°, −6°, −4°, −2°, 0°, +2°, +4°, +6°, +8°

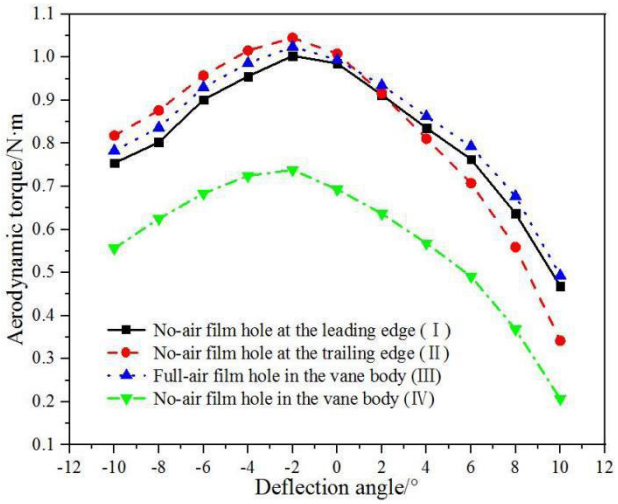

FIGURE 26. The relationship between aerodynamic torque and deflection angle at different air film hole distributions.

and +10° at 4%, 8% and 12% flow ratios. Figure 25 shows the relationship between friction torque and deflection angle at different flow ratios. It can be seen from Table 9 and Figure 25 that at the flow ratios of 4%, 8% and 12%, the friction torque of the guide vane decreases with the deflection angle. At the deflection angle -10°, the friction torque reaches the maximum value. The friction torques are 2.73135N·m, 2.70744N·m and 2.69270N·m for the flow ratios of 4%, 8% and 12%, respectively. At the deflection angle +10°, the friction torque reaches the minimum value. The friction torques are 2.35275N·m, 2.33004N·m and 2.31268N·m for the flow ratios of 4%, 8% and 12%, respectively. And with the flow ratio increasing, the friction torque of the guide vane slightly decreases. At the same deflection angle, the friction torques of 4%, 8% and 12% flow ratios decrease sequentially.

I. ANALYSIS OF AERODYNAMIC TORQUE AND FRICTION TORQUE WITH DIFFERENT AIR FILM HOLE DISTRIBUTIONS

Combined with UDF program operation, the aerodynamic torque of the guide vane is calculated. Table 10 shows the aerodynamic torque at different air film hole distributions. Table 10 gives the aerodynamic torques of the guide vane for the deflection angles of −10°, −8°, −6°, −4°, −2°, 0°, +2°, +4°, +6°, +8° and +10° at the four distributions of no-air film hole at the leading edge (case I), no-air film hole at the trailing edge (case II), full-air film hole in the vane body (case III) and no-air film hole in the vane body (case IV) respectively. Figure 26 shows the relationship between aerodynamic torque and deflection angle at different air film hole distributions. From Table 10 and Figure 26, it can be seen that at the four distributions of case I, case II, case III and case IV, the aerodynamic torque of the guide vane first increases and then decreases with the deflection angle. At the deflection angle −2°, the aerodynamic torque reaches the maximum value. The aerodynamic torques are 1.00316N·m, 1.04475N·m, 1.02416N·m and 0.738359N·m for the four distributions of

TABLE 10. Aerodynamic torque of different air film hole distributions.

Deflection angle[°]	Aerodynamic torque[N·m]			
	No-air film hole at the leading edge (case I)	No-air film hole at the trailing edge (case II)	Full-air film hole in the vane body (case III)	No-air film hole in the vane body (case IV)
-10	0.754286	0.817860	0.783108	0.556476
-8	0.802527	0.876392	0.836514	0.625091
-6	0.901284	0.957363	0.929963	0.683748
-4	0.955366	1.01534	0.985836	0.724829
-2	1.00316	1.04475	1.02416	0.738359
0	0.985280	1.00797	0.993760	0.693107
+2	0.912353	0.915810	0.934746	0.637078
+4	0.835741	0.810628	0.862730	0.567983
+6	0.762940	0.707523	0.792776	0.490940
+8	0.637180	0.558960	0.677382	0.368478
+10	0.468576	0.341739	0.493313	0.207330

case I, case II, case III and case IV, respectively. At the deflection angle +10°, the aerodynamic torque reaches the minimum value. The aerodynamic torques are 0.468576N·m, 0.341739N·m, 0.493313N·m and 0.207330N·m for the four distributions of case I, case II, case III and case IV, respectively. And in the range of -10° to 0°, with the same deflection angle, the aerodynamic torque of case II is the biggest. The aerodynamic torque of case IV is the smallest. The aerodynamic torques of case I, case II, case III and case IV decrease sequentially. However, in the range of 0° to +10°, with the same deflection angle, the aerodynamic torque of case III is the biggest. The aerodynamic torque of case IV is the smallest. The aerodynamic torques of case I, case II, case III and case IV decrease sequentially.

Combined with UDF program operation, the friction torque of the guide vane is calculated. Table 11 shows the friction torque at different air film hole distributions. Table 11 gives the friction torques of the guide vane for the deflection angles of −10°, −8°, −6°, −4°, −2°, 0°, +2°, +4°, +6°, +8° and +10° at the four distributions of no-air film hole at the leading edge (case I), no-air film hole at the trailing edge (case II), full-air film hole in the vane body (case III) and no-air film hole in the vane body (case IV) respectively. Figure 27 shows the relationship between friction torque and deflection angle at different air film hole distributions. From Table 11 and Figure 27, it can be seen that at the four distributions of case I, case II, case III and case IV, the friction torque of the guide vane decreases with the deflection angle.

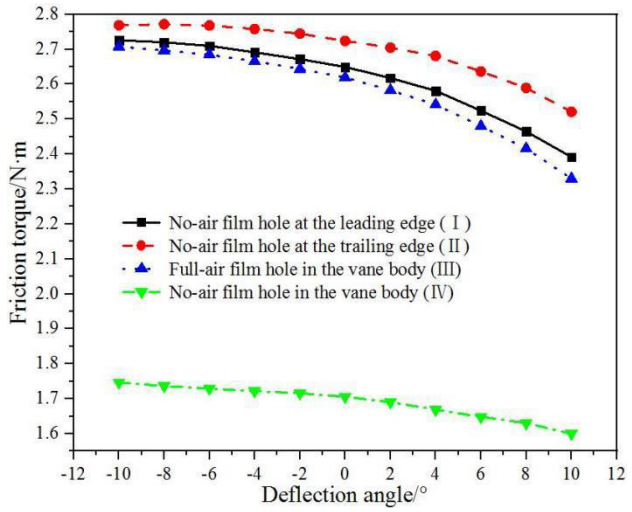

FIGURE 27. The relationship between friction torque and deflection angle at different air film hole distributions.

TABLE 11. Friction torque of different air film hole distributions.

Deflection angle[°]	Friction torque[N·m]			
	No-air film hole at the leading edge (case Ⅰ)	No-air film hole at the trailing edge (case Ⅱ)	Full-air film hole in the vane body (case Ⅲ)	No-air film hole in the vane body (case Ⅳ)
-10	2.72555	2.76859	2.70744	1.74671
-8	2.71962	2.77147	2.69663	1.73650
-6	2.70958	2.76772	2.68420	1.72925
-4	2.69101	2.75780	2.66559	1.72197
-2	2.67152	2.74455	2.64366	1.71579
0	2.64924	2.72352	2.61894	1.70580
+2	2.61751	2.70435	2.58254	1.69028
+4	2.58103	2.68043	2.54138	1.66897
+6	2.52427	2.63622	2.47994	1.64826
+8	2.46482	2.58934	2.41582	1.63034
+10	2.39151	2.52079	2.33004	1.59999

At the deflection angle −10°, the friction torque reaches the maximum value. The friction torques are 2.72555N·m, 2.76859N·m, 2.70744N·m and 1.74671N·m for the four distributions of case I, case II, case III and case IV, respectively. At the deflection angle +10°, the friction torque reaches the minimum value. The friction torques are 2.39151N·m, 2.52079N·m, 2.33004N·m and 1.59999N·m for the four distributions of case I, case II, case III and case IV, respectively. And in the range of −10° to +10°, with the same deflection angle, the friction torque of case II is the biggest. The friction torque of case IV is the smallest. The friction torques of case I, case II, case III and case IV decrease sequentially.

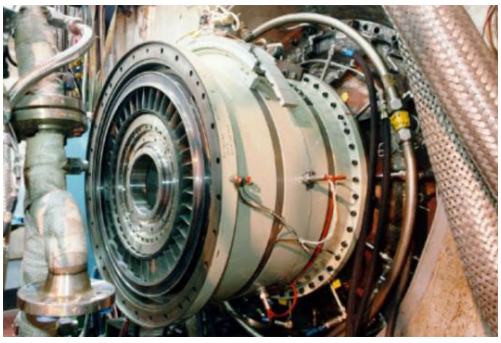

FIGURE 28. Variable geometry turbine of variable cycle engine.

TABLE 12. Resultant torque of different air film hole distributions.

Deflection angle[°]	Resultant torque[N·m]			
	No-air film hole at the leading edge (case Ⅰ)	No-air film hole at the trailing edge (case Ⅱ)	Full-air film hole in the vane body (case Ⅲ)	No-air film hole in the vane body (case Ⅳ)
-10	3.479836	3.58645	3.490548	2.303186
-8	3.522147	3.647862	3.533144	2.361591
-6	3.610864	3.725083	3.614163	2.354341
-4	3.646376	3.77314	3.651426	2.446799
-2	3.67468	3.7893	3.66782	2.454149
0	3.63452	3.73149	3.6127	2.398907
+2	3.529863	3.62016	3.517286	2.327358
+4	3.416771	3.491058	3.40411	2.236953
+6	3.28721	3.343743	3.272716	2.1392
+8	3.102	3.1483	3.093202	1.998818
+10	2.860086	2.862529	2.823353	1.80732

J. ANALYSIS OF RESULTANT TORQUE WITH DIFFERENT AIR FILM HOLE DISTRIBUTIONS

Combined with UDF program operation, the resultant torque of the guide vane is calculated. Figure 28 shows the variable geometry turbine of a variable cycle engine. Table 12 shows the resultant torque at different air film hole distributions. Table 12 gives the resultant torques of the guide vane for the deflection angles of −10°, −8°, −6°, −4°, -2°, 0°, +2°, +4°, +6°, +8° and +10° at the four distributions of no-air film hole at the leading edge (case I), no-air film hole at the trailing edge (case II), full-air film hole in the vane body

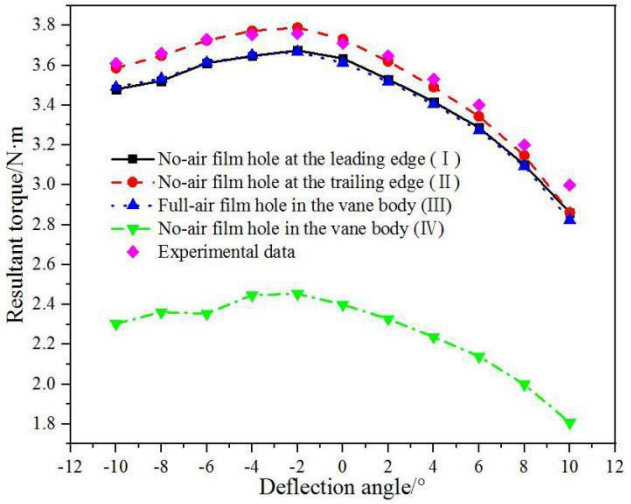

FIGURE 29. The relationship between resultant torque and deflection angle at different air film hole distributions.

(case III) and no-air film hole in the vane body (case IV) respectively. Figure 29 shows the relationship between resultant torque and deflection angle at different air film hole distributions. From Table 12 and Figure 29, it can be seen that at the four distributions of case I, case II, case III and case IV, the resultant torque of the guide vane first increases and then decreases with the deflection angle. At the deflection angle $-2°$, the resultant torque reaches the maximum value. The resultant torques are 3.67468N·m, 3.7893N·m, 3.66782N·m and 2.454149N·m for the four distributions of case I, case II, case III and case IV, respectively. At the deflection angle $+10°$, the resultant torque reaches the minimum value. The resultant torques are 2.860086N·m, 2.862529N·m, 2.823353N·m and 1.80732N·m for the four distributions of case I, case II, case III and case IV, respectively. And in the range of $-10°$ to $-4°$, with the same deflection angle, the resultant torque of case II is the biggest. The resultant torque of case IV is the smallest. The resultant torques of case I, case II, case III and case IV decrease sequentially. However, in the range of $-2°$ to $+10°$, with the same deflection angle, the resultant torque of case II is the biggest. The resultant torque of case IV is the smallest. The resultant torques of case I, case II, case III and case IV decrease sequentially. At the same time, the research institute provided experimental data of the resultant torque. The result indicates that the coupling calculation results are in good agreement with the experimental data. The numerical simulation results have high reliability. It is feasible to provide the required torque for the design of variable geometry turbine adjusting mechanisms.

From Table 12 and Figure 29, it can be seen that the research institute provided experimental data of the resultant torque. At the deflection angle $-2°$, the resultant torque reaches the maximum value. The numerical calculation result of full-air film hole in the vane body (case III) is 3.66782N·m, and the resultant torque of the experimental data is 3.7601N·m. At the deflection angle $+10°$, the resultant torque reaches the minimum value. The numerical calculation result of full-air film hole in the vane body (case III) is 2.823353N·m, and the resultant torque of the experimental data is 3.0245N·m. At the deflection angle $-10°$, the numerical calculation result of full-air film hole in the vane body (case III) is 3.490548N·m, and the resultant torque of the experimental data is 3.6104N·m. The differences between the numerical calculation results and the experimental data are 3.319%, 2.454% and 6.651% for the deflection angles of $-10°$, $-2°$, $+10°$, respectively. The above comparisons verify the accuracy of the numerical calculation method applied in the study of guide vane torque in the article.

IV. CONCLUSION

This article studies three influencing factors on the torque of the rotating guide vane of the variable geometry turbine guide vane adjusting mechanism in a variable cycle engine. At the guide vane deflection angles of $-10°$, $-8°$, $-6°$, $-4°$, $-2°$, $0°$, $+2°$, $+4°$, $+6°$, $+8°$ and $+10°$, the targets are the effects of turbulence intensity, flow ratio and air film hole distribution on the guide vane torque. CFD temperature–fluid–solid coupling algorithm and UDF program are used to solve the torque of the guide vane shaft. The calculation results were compared with the experimental data provided by the research institute. The following conclusions have been drawn.

1) The temperature distribution of the pressure and suction surfaces of the guide vanes clearly shows a gradient distribution change. And the surface of the guide vanes is well cooled by the air film. There will be a significant temperature gradient at the leading and trailing edges of the blade. There is a significant thermal stress. This is consistent with the location where ablation is prone to occur in the actual operation of the turbine guide vanes. The pressure distribution on the pressure and suction surfaces of the guide vanes clearly shows a gradient distribution change. A distinct low-pressure area appears after each air-exhaust film holes. That is, a sudden drop in pressure. This leads to oscillations in the pressure in front of and behind the air film holes. This causes the guide vanes to be subjected to high lateral pressure. It generates aerodynamic and friction torque at the rotating shaft of the guide vane. And the maximum velocity of the flow field increases with increasing deflection angle. The maximum velocities of the flow field are 522.5m/s, 534.4m/s and 600.8m/s for the guide vane deflection angles of $-10°$, $0°$ and $+10°$, respectively.
2) At 1%, 5% and 10% turbulence intensities, the aerodynamic torque of the guide vane first increases and then decreases with the deflection angle. At the deflection angle $-2°$, the aerodynamic torque reaches the maximum value. The aerodynamic torques are 1.08067N·m,

1.07129N·m and 1.06198N·m for the turbulence intensities of 1%, 5% and 10%, respectively. At the deflection angle +10°, the aerodynamic torque reaches the minimum value. The aerodynamic torques are 0.544089N·m, 0.533761N·m and 0.523507N·m for the turbulence intensities of 1%, 5% and 10%, respectively. And with the turbulence intensity increasing, the aerodynamic torque of the guide vane slightly decreases. At the same deflection angle, the aerodynamic torques of 1%, 5% and 10% turbulence intensities decrease sequentially. At the turbulence intensities of 1%, 5% and 10%, the friction torque of the guide vane decreases with the deflection angle. At the deflection angle −10°, the friction torque reaches the maximum value. The friction torques are 2.74186N·m, 2.73135N·m and 2.72179N·m for the turbulence intensities of 1%, 5% and 10%, respectively. At the deflection angle +10°, the friction torque reaches the minimum value. The friction torques are 2.36145N·m, 2.35275N·m and 2.34388N·m for the turbulence intensities of 1%, 5% and 10%, respectively. And with the turbulence intensity increasing, the friction torque of the guide vane slightly decreases. At the same deflection angle, the friction torques of 1%, 5% and 10% turbulence intensities decrease sequentially.

3) At 4%, 8% and 12% flow ratios, the aerodynamic torque of the guide vane first increases and then decreases with the deflection angle. At the deflection angle −2°, the aerodynamic torque reaches the maximum value. The aerodynamic torques are 1.07167N·m, 1.02416N·m and 0.948665N·m for the flow ratios of 4%, 8% and 12%, respectively. At the deflection angle +10°, the aerodynamic torque reaches the minimum value. The aerodynamic torques are 0.533761N·m, 0.493313N·m and 0.441955N·m for the flow ratios of 4%, 8% and 12%, respectively. And with the flow ratio increasing, the aerodynamic torque of the guide vane slightly decreases. At the same deflection angle, the aerodynamic torques of 4%, 8% and 12% flow ratios decrease sequentially. At the flow ratios of 4%, 8% and 12%, the friction torque of the guide vane decreases with the deflection angle. At the deflection angle −10°, the friction torque reaches the maximum value. The friction torques are 2.73135N·m, 2.70744N·m and 2.69270N·m for the flow ratios of 4%, 8% and 12%, respectively. At the deflection angle +10°, the friction torque reaches the minimum value. The friction torques are 2.35275N·m, 2.33004N·m and 2.31268N·m for the flow ratios of 4%, 8% and 12%, respectively. And with the flow ratio increasing, the friction torque of the guide vane slightly decreases. At the same deflection angle, the friction torques of 4%, 8% and 12% flow ratios decrease sequentially.

4) At the four distributions of case I, case II, case III and case IV, the aerodynamic torque of the guide vane first increases and then decreases with the deflection angle. And in the range of −10° to 0°, with the same deflection angle, the aerodynamic torque of case II is the biggest. The aerodynamic torque of case IV is the smallest. The aerodynamic torques of case I, case II, case III and case IV decrease sequentially. However, in the range of 0° to +10°, with the same deflection angle, the aerodynamic torque of case III is the biggest. The aerodynamic torque of case IV is the smallest. The aerodynamic torques of case I, case II, case III and case IV decrease sequentially. At the four distributions of case I, case II, case III and case IV, the friction torque of the guide vane decreases with the deflection angle. And in the range of −10° to +10°, with the same deflection angle, the friction torque of case II is the biggest. The friction torque of case IV is the smallest. The friction torques of case I, case II, case III and case IV decrease sequentially.

At the four distributions of case I, case II, case III and case IV, the resultant torque of the guide vane first increases and then decreases with the deflection angle. At the deflection angle −2°, the resultant torque reaches the maximum value. The resultant torques are 3.67468N·m, 3.7893N·m, 3.66782N·m and 2.454149N·m for the four distributions of case I, case II, case III and case IV, respectively. At the deflection angle +10°, the resultant torque reaches the minimum value. The resultant torques are 2.860086N·m, 2.862529N·m, 2.823353N·m and 1.80732N·m for the four distributions of case I, case II, case III and case IV, respectively. And in the range of −10° to −4°, with the same deflection angle, the resultant torque of case II is the biggest. The resultant torque of case IV is the smallest. The resultant torques of case I, case II, case III and case IV decrease sequentially. However, in the range of −2° to +10°, with the same deflection angle, the resultant torque of case II is the biggest. The resultant torque of case IV is the smallest. The resultant torques of case I, case II, case III and case IV decrease sequentially. At the same time, the research institute provided experimental data of the resultant torque. The result indicates that the coupling calculation results are in good agreement with the experimental data. The numerical simulation results have high reliability. It is feasible to provide the required torque for the design of variable geometry turbine adjusting mechanisms.

DATA AVAILABILITY STATEMENT

The data presented in this study are available on demand from the first author at (zhongyan524@163.com).

CONFLICTS OF INTEREST

The authors declared no potential conflicts of interest with respect to the research, authorship and/or publication of this article.

REFERENCES

[1] J. D. Denton and W. N. Dawes, "Computational fluid dynamics for turbomachinery design," *Proc. Inst. Mech. Eng., C, J. Mech. Eng. Sci.*, vol. 213, pp. 107–124, Feb. 1998.

[2] S. Wei and Z. Kun, "Design method for high ma number counter rotating turbine blades," in *Proc. Turbomachinery*, vol. 2B. Montreal, QC, Canada, Jun. 2015, pp. 15–19.

[3] M. P. Boyce, *Gas Turbine Engineering Handbook*. Amsterdam, The Netherlands: Elsevier, 2011, pp. 841–842.

[4] Y. Li and Z. Wang, "Aero-engine guide vane angle regulator iterative learning control method," in *Proc. IEEE 3rd Adv. Inf. Technol., Electron. Autom. Control Conf. (IAEAC)*, Chongqing, China, Oct. 2018, pp. 2401–2405, doi: 10.1109/IAEAC.2018.8577536.

[5] W. Zhao, L. Wang, Z. Zhai, and Z. Wang, "Application of multi-objective optimized methods in the closing law of guide vanes," in *Proc. Chin. Control Decis. Conf.*, May 2010, pp. 3552–3556, doi: 10.1109/CCDC.2010.5498553.

[6] V. Obretenov and R. Iliev, "Determination of the optimal parameters of a vertical axis wind turbine with cylindrical guide vane unit," in *Proc. 6th Int. Symp. Environ.-Friendly Energies Appl. (EFEA)*, Sofia, Bulgaria, Mar. 2021, pp. 1–5, doi: 10.1109/EFEA49713.2021.9406245.

[7] K. Ananthakrishnan and M. Govardhan, "Effect of constant and variable radii fillet on secondary flow field of transonic turbine stage's nozzle guide vane," in *Proc. 7th Int. Conf. Mech. Aerosp. Eng. (ICMAE)*, Jul. 2016, pp. 543–548, doi: 10.1109/ICMAE.2016.7549599.

[8] P. R. Kukutla and B. V. S. S. S. Prasad, "Flow analysis of combined impingement and film cooled gas turbine nozzle guide vane," in *Proc. IEEE Aerosp. Conf.*, Big Sky, MT, USA, Mar. 2016, pp. 1–20, doi: 10.1109/AERO.2016.7500843.

[9] K. Peng, J. Fu, D. Fan, and L. Zhang, "Improved genetic algorithm and its application in parameter optimization for certain aeroengine compressor guide vane regulator," in *Proc. Int. Conf. Electron., Commun. Control (ICECC)*, Ningbo, China, Sep. 2011, pp. 2097–2100, doi: 10.1109/ICECC.2011.6067789.

[10] S. Nižetic, Ž. Penga, and M. Arici, "Influence of guide vane topology on the shape and stability of gravitational vortex," in *Proc. 3rd Int. Conf. Smart Sustain. Technol. (SpliTech)*, Split, Croatia, Jun. 2018, pp. 1–6.

[11] M. Hu, M. Chen, W. H. Chen, Y. P. Jin, J. Pan, and M. M. Zhang, "Kinematics analysis and basic parameters design on the rotating-guide-bar and gear mechanisms assembled driving systems of differential velocity vane pump," in *Proc. IEEE Int. Conf. Mechatronics Autom.*, Aug. 2010, pp. 1220–1223, doi: 10.1109/ICMA.2010.5588121.

[12] N. Gupta, A. Kumar, S. Banerjee, and S. Jha, "Magnetically levitated VAWT with closed loop wind speed conditioning guide vanes," in *Proc. IEEE 1st Int. Conf. Power Electron., Intell. Control Energy Syst. (ICPEICES)*, Delhi, India, Jul. 2016, pp. 1–5, doi: 10.1109/ICPEICES.2016.7853126.

[13] Y. Zhang, S. Liu, J. Liu, and Y. Wu, "Numerical simulation of flow characteristics of pump turbine with small guide vanes opening," in *Proc. ISFMFE 6th Int. Symp. Fluid Machinery Fluid Eng.*, Oct. 2014, pp. 1–6, doi: 10.1049/cp.2014.1131.

[14] Y. Ding, Y. Liu, and J. Niu, "Numerical simulation of heat transfer distribution over the surface of internally cooled nozzle guide vane in an annular cascade," in *Proc. IEEE Int. Conf. Mechatronics Autom. (ICMA)*, Takamatsu, Japan, Aug. 2017, pp. 1906–1911, doi: 10.1109/ICMA.2017.8016109.

[15] B. Cheng and D. Sakaguchi, "Optimization of a recirculation flow type casing treatment with guide vanes for centrifugal compressors," in *Proc. 5th Int. Conf. Control, Autom. Robot. (ICCAR)*, Beijing, China, Apr. 2019, pp. 702–707, doi: 10.1109/ICCAR.2019.8813477.

[16] Y. Xu, Q. Zhang, W. Shi, W. Lu, C. Wang, and L. Zhou, "Performance analysis of a new axial guide vane based on numerical simulations," in *Proc. ISFMFE 6th Int. Symp. Fluid Machinery Fluid Eng.*, Oct. 2014, pp. 1–7, doi: 10.1049/cp.2014.1141.

[17] T. Zeng, D. Upadhyay, H. Sun, and G. G. Zhu, "Physics-based turbine power models for a variable geometry turbocharger," in *Proc. Amer. Control Conf. (ACC)*, Boston, MA, USA, Jul. 2016, pp. 5099–5104, doi: 10.1109/ACC.2016.7526162.

[18] Y. Zeng-Ming and Z. Ting-Ting, "Research of guide vane proposals for the single-stage axial-flow fans used in the large generator," in *Proc. Int. Conf. Sustain. Power Gener. Supply*, Nanjing, China, Apr. 2009, pp. 1–4, doi: 10.1109/SUPERGEN.2009.5348150.

[19] M. Tong and T. Tong, "Research of thermal stress on a high pressure turbine guide vane during the start-up period," in *Proc. 8th Int. Conf. Mech. Eng. Autom. Sci. (ICMEAS)*, Wuhan, China, Oct. 2022, pp. 287–294, doi: 10.1109/ICMEAS57305.2022.00061.

[20] Z. Fei, D. Xiaohui, X. Bin, and B. Yuxing, "Research on pressure fluctuation in impeller and guide vane of boiler water circulating pump," in *Proc. 2nd Int. Conf. Power Renew. Energy (ICPRE)*, Chengdu, China, Sep. 2017, pp. 786–790, doi: 10.1109/ICPRE.2017.8390641.

[21] L. Xiao, R. Gong, X. Fan, and Y. Zhu, "Sliding mode control for turboshaft engine with variable inlet guide vane," in *Proc. 11th World Congr. Intell. Control Autom.*, Shenyang, China, Jun. 2014, pp. 3972–3976, doi: 10.1109/WCICA.2014.7053380.

[22] H. Jianjun, Z. Dun, R. Yan, and Z. Yuan, "Study on hydraulic characteristics of tubular pump guide vanes," in *Proc. Int. Conf. Mater. Renew. Energy Environ.*, vol. 2, May 2011, pp. 1902–1906, doi: 10.1109/ICMREE.2011.5930709.

[23] S.-Y. Peng, Z.-G. Li, J.-R. Zhang, Y.-Z. Zhao, L. Wang, D.-M. Liu, J.-M. Yang, and B.-Q. Yang, "The working conditions optimization of low-head water turbine with different guide vane outlet angle," in *Proc. IEEE Innov. Smart Grid Technol. Asia (ISGT Asia)*, Chengdu, China, May 2019, pp. 4268–4273, doi: 10.1109/ISGT-Asia.2019.8881116.

[24] M. M. A. Alam, M. Takao, A. Takami, S. Okuhara, Y. Kinoue, and T. Setoguchi, "Wells turbine with booster—Effect of guide vanes on the performance-," in *Proc. IEEE Int. Conf. Renew. Energy Res. Appl. (ICRERA)*, Nov. 2016, pp. 189–192, doi: 10.1109/ICRERA.2016.7884535.

[25] K. Touil and A. Ghenaiet, "Simulation and analysis of vane-blade interaction in a two-stage high-pressure axial turbine," *Energy*, vol. 172, pp. 1291–1311, Apr. 2019.

[26] X. Chen, W. Chu, G. Wang, S. Yan, Z. Shen, and Z. Guo, "Effect of span range of variable-camber inlet guide vane in an axial compressor," *Aerosp. Sci. Technol.*, vol. 116, Sep. 2021, Art. no. 106836, doi: 10.1016/j.ast.2021.106836.

[27] C. Chen, C. Han, S. Peng, and Z. C. Chun, "An aerodynamic calculation model for anti-torque system of NOTOR," *Mechanics*, vol. 24, no. 2, pp. 213–220, May 2018, doi: 10.5755/j01.mech.24.2.19740.

YAN ZHONG received the bachelor's and master's degrees in mechanical engineering and automation from the Liaoning University of Science and Technology, Anshan, China, in 2009 and 2014, respectively. He is currently pursuing the Ph.D. degree in mechanical engineering and automation with Northeastern University, Shenyang, China. His research interests include mechanics of plate and strip rolling, experimental study on warm rolling of magnesium alloy plate and strip, and research on variable geometry turbine guide vane adjusting mechanism.

LIANGYU CHEN was born in 1959. He is currently a Professor. He was selected as a talent at the level of 100 people in the "Hundred, Thousand, and Ten Thousand Talent Project" in Liaoning Province. He is enjoying special allowances from the State Council. He has undertaken and completed over 30 National Natural Science Foundation and various science and technology projects. He has published seven monographs and books. He has published over 50 articles. His research interests include modern mechanical transmission, engineering structural modeling and digital design, and structural integrity of metallurgical thermal furnaces and kilns. He has won ten awards for various scientific and technological progress.

LEI ZHAO received the B.S. degree in mechanical engineering from Zaozhuang University, Shandong, China, in 2017, and the M.S. degree in mechanical engineering from the University of Science and Technology Liaoning, Anshan, China, in 2020. He is currently pursuing the Ph.D. degree in power engineering with Northeastern University, China. His research interests include granular matter dynamics and application of discrete element method in engineering machinery.

LEI WANG was born in Anshan, Liaoning, China, in 1994. He received the B.Eng. degree in mechanical design manufacture and automation from Shenyang Agricultural University, Shenyang, China, in 2017, and the M.Eng. degree in mechanical engineering from Northeastern University, Shenyang, in 2019, where he is currently pursuing the Ph.D. degree in mechanical engineering. His research interests include the safety evaluation of blast furnace hearth structure and thermal stress of blast furnace hearth.

ZHUO YAN received the bachelor's and master's degrees in mechanical engineering from Northeastern University, Shenyang, China, in 2018 and 2021, respectively. He is currently the Designer with the FAW Jiefang Commercial Vehicle Development Institute. His research interests include vehicle module design, frame structure design of new energy gas electric vehicle models, and static strength analysis of the frame.

HAOXI BAI received the bachelor's degree in mechanical engineering and automation from the Liaoning University of Engineering and Technology, in 2018, and the master's degree in mechanical engineering from Northeastern University, Shenyang, China, in 2021. She is currently the Designer of TBEA Shenyang Transformer Group Company Ltd. Her research interests include transformer structural design and research on variable geometry turbine guide vane adjusting mechanism.